

# Antagonistic cell surface and intracellular auxin signalling regulate plasma membrane H<sup>+</sup>-fluxes for root growth

**Authors:** Lanxin Li<sup>†1</sup>, Inge Verstraeten<sup>†1</sup>, Mark Roosjen<sup>2</sup>, Koji Takahashi<sup>3,4</sup>, Lesia Rodriguez<sup>1</sup>, Jack Merrin<sup>1</sup>, Jian Chen<sup>5,6</sup>, Lana Shabala<sup>7</sup>, Wouter Smet<sup>5,6</sup>, Hong Ren<sup>8</sup>, Steffen Vanneste<sup>5,9,10</sup>, Sergey Shabala<sup>7,11</sup>, Bert De Rybel<sup>5,6</sup>, Dolf Weijers<sup>2</sup>, Toshinori Kinoshita<sup>3,4</sup>, William M. Gray<sup>8</sup> and Jiří Friml<sup>1</sup>

## Affiliations:

<sup>1</sup> Institute of Science and Technology (IST) Austria – 3400 Klosterneuburg (Austria).

<sup>2</sup> Department of Agrotechnology and Food Sciences, Laboratory of Biochemistry, Wageningen University – 6708 WE Wageningen (the Netherlands).

<sup>3</sup> Institute of Transformative Bio-Molecules, Nagoya University, Division of Biological Science – 464-8602 Chikusa Nagoya (Japan).

<sup>4</sup> Graduate School of Science, Nagoya University – 464-8602 Chikusa Nagoya (Japan).

<sup>5</sup> Ghent University, Department of Plant Biotechnology and Bioinformatics – 9052 Gent (Belgium).

<sup>6</sup> VIB Center for Plant Systems Biology – 9052 Gent (Belgium).

<sup>7</sup> Tasmanian Institute of Agriculture, College of Science and Engineering, University of Tasmania – Hobart (Australia).

<sup>8</sup> Department of Plant & Microbial Biology, University of Minnesota – MN-55108, St. Paul (United States).

<sup>9</sup> Lab of Plant Growth Analysis, Ghent University Global Campus – Incheon 21985 (Republic of Korea)

<sup>10</sup> Department of Plants and Crops – HortiCell, Ghent University – 9000 Gent (Belgium).

<sup>11</sup> International Research Centre for Environmental Membrane Biology, Foshan University – 528000 Foshan (China)

\*Correspondence to: [jiri.friml@ist.ac.at](mailto:jiri.friml@ist.ac.at)

† These authors contributed equally to this work

## Abstract

Growth regulation tailors plant development to its environment. A showcase is growth adaptation to gravity, where shoots bend up and roots down. This paradox is based on different responses to the phytohormone auxin, which promotes cell expansion in shoots, while inhibiting it in roots via a yet unknown cellular mechanism. Here, by combining microfluidics, live imaging, genetic engineering and phospho-proteomics in *Arabidopsis thaliana*, we reveal how auxin inhibits root growth. We show that auxin activates two distinct, antagonistically acting signalling pathways that converge on the rapid regulation of the apoplastic

pH, which is the direct growth-determining mechanism. Cell surface-based TRANSMEMBRANE KINASE 1 (TMK1) interacts with and mediates phosphorylation and activation of plasma membrane H<sup>+</sup>-ATPases for apoplast acidification, while intracellular TIR1/AFB-mediated signalling triggers net cellular H<sup>+</sup>-influx, causing apoplast alkalinisation. The simultaneous activation of these two counteracting mechanisms poises the root for a rapid, fine-tuned growth modulation to subtle changes in the environment.

## Main

Auxin, as a major growth regulator in plants, acts oppositely in shoots and roots. In shoots, it promotes cell elongation by activating H<sup>+</sup>-pumps to acidify the apoplast<sup>1</sup> in agreement with the classical Acid Growth Theory, which postulates that low apoplastic pH promotes growth<sup>2-4</sup>. This relatively slow process relies on the canonical/intracellular TIR1/AFB receptors-mediated pathway of transcriptional regulation<sup>5-7</sup>. In many species including the model *Arabidopsis*, however, auxin inhibits growth in roots<sup>8</sup> by an unclear cellular mechanism. This contrasting response to the same signal is the basis for the positive versus negative bending of roots and shoots in response to gravity and light. The inhibitory auxin effect in roots is very rapid, but also involves TIR1/AFB receptors<sup>9</sup>. The timing indicates the existence of a rapid, non-transcriptional branch of this pathway<sup>9</sup>, nonetheless with unclear downstream molecular, cellular and physiological mechanisms. Besides intracellular TIR1/AFB auxin signalling, a cell surface-based pathway mediated by TRANSMEMBRANE KINASE 1 (TMK1) has been shown to regulate differential growth in the apical hook<sup>10</sup>, while its contribution to a general growth regulation, remains unclear. Hence, the auxin signalling mechanism and the downstream cellular mechanisms for regulating root growth remain elusive.

In this study, we revealed simultaneous antagonistic activities of TIR1/AFB intracellular and TMK1-based cell surface auxin signalling converging on regulation of apoplastic pH, which we identified as the key cellular mechanism allowing immediate and sensitive root growth regulation.

## Auxin-induced root growth inhibition correlates with a rapid increase in apoplastic pH

Auxin rapidly and non-transcriptionally inhibits root growth through TIR1/AFB auxin signalling<sup>9</sup>. Although several processes, including cortical microtubule (CMT) reorientation<sup>11,12</sup>, vacuolar fragmentation<sup>13</sup> and apoplastic pH changes<sup>14-16</sup> are implicated, the causal mechanism mediating rapid auxin inhibition of root growth remains unidentified.

The microfluidic vRootchip<sup>9</sup> setup in combination with vertical confocal microscopy<sup>17</sup> allowed us to critically re-evaluate the contributions of these processes by comparing their kinetics. Growth inhibition was observed within 30 seconds after 10 nM of the natural auxin indole-3-acetic acid (IAA)<sup>9</sup>. Using the microtubule plus-end marker *pEB1b::EB1b-GFP*, we observed that even using 100 nM IAA, less than 5% of the CMT in elongating epidermal cells reoriented after 1 minute (Extended Data Fig. 1a-b). Furthermore,

inhibition of CMT dynamics by taxol treatment blocked auxin-mediated CMT reorientation (Extended Data Fig. 1c-d), but had no effect on auxin-mediated growth inhibition (Extended Data Fig. 1e). We visualized vacuolar morphology using tonoplast marker *pSYP22::SYP22-YFP*. By live imaging the same cells, we could not detect obvious changes in vacuolar morphology even after 30 minutes of 100 nM IAA treatment (Extended Data Fig. 1f), when root growth was already strongly inhibited. These results show that both CMT reorientation and vacuole constriction occur well after the rapid auxin-mediated growth inhibition, arguing against their involvement in this process.

To evaluate the kinetics of apoplastic pH changes, we applied a membrane-impermeable ratiometric pH indicator: 8-hydroxypyrene-1,3,6-trisulfonic acid (HPTS)<sup>14</sup> and imaged apoplastic pH in elongating epidermis cells while simultaneously tracking root tip growth in the vRootchip. We detected a gradient in the apoplastic pH, decreasing from transition to elongation zone, in root epidermal cells (Extended Data Fig. 1g). Regardless of their position, all cells showed a strong apoplastic pH increase within 30 seconds of 5 nM IAA treatment (Fig. 1a, b and Extended Data Fig. 1g). This auxin-mediated alkalinisation was observed at the same time as root growth inhibition (Fig. 1b). The pH increase was very robust as we also detected alkalinisation of the external medium along the root tip surface (Extended Data Fig. 1h). In a complementary approach, we analysed the cytosolic pH by using the PM-Cyto reporter<sup>18</sup>. The cytosolic pH adjacent to the PM decreased within 30 seconds of 5 nM IAA treatment (Fig. 1c). The concomitant apoplastic pH increase and intracellular decrease in elongating root epidermal cells suggest that auxin causes a H<sup>+</sup>-influx into the cell. This notion was confirmed in direct experiments using non-invasive ion microelectrodes monitoring the net H<sup>+</sup>-exchange across the PM of root elongating epidermis cells (Extended Data Fig. 1i).

Overall, auxin triggers rapid apoplast alkalinisation by increasing the net H<sup>+</sup>-flux into cells. Strong spatial and temporal correlation with auxin-mediated root growth inhibition suggests that apoplast alkalinisation may be the key cellular mechanism, by which auxin rapidly inhibits root growth.

### **Apoplastic pH is causative for rapid root growth regulation**

To investigate the causal relationship between apoplast alkalinisation and root growth inhibition, we manipulated the apoplastic pH by changing the pH of the medium and monitoring the impact on root growth using the vRootchip. Indeed, pH manipulation of the medium had a rapid impact on the root apoplastic pH (Extended Data Fig. 1j-k). Replacement of the standard medium at pH 5.8 by a more alkaline (pH 6.15) medium caused instant reduction of root growth; the growth rate restored rapidly after washout with the original pH 5.8 medium (Fig. 1d, e). Gradual alkalinisation of the medium resulted in gradual root growth inhibition (Extended Data Fig. 1l). On the other hand, replacing the alkaline medium by more acidic pH 5.1 medium increased root growth instantly and washout restored the original growth rate (Fig. 1f, g).

Thus, exogenous manipulation of apoplastic pH has an immediate and reversible effect on root growth, with alkaline pH inhibiting and acidic pH promoting growth. This resembles the root growth inhibition effects of auxin in both speed and reversibility and strongly supports that auxin-induced apoplast alkalisation is the key downstream cellular mechanism for rapid root growth inhibition.

### **Auxin rapidly phosphorylates and activates plasma membrane H<sup>+</sup>-ATPases in the root**

The auxin effect on apoplast alkalisation occurs within seconds, thus being too fast to involve transcriptional regulation. To gain insights into the underlying mechanism, we mined recent datasets from Mass Spectroscopy (MS)-aided phospho-proteomics in *Arabidopsis* root tips treated for 2 minutes with 100 nM IAA (Han et al., manuscript in preparation). Among the top differentially phosphorylated targets were two Plasma Membrane (PM) H<sup>+</sup>-ATPases encoded by AT2G18960 (AHA1) and AT4G30190 (AHA2). Multiple putative phosphorylation sites were identified in the auto-inhibitory C-terminal region as being regulated by auxin, potentially leading to both activation and deactivation of H<sup>+</sup>-pump activity<sup>19,20</sup> (Fig. 2a and Extended Data Table 1). This suggested that auxin may regulate H<sup>+</sup>-pump activity in roots via phosphorylation, providing a plausible mechanism for the observed rapid auxin effect on apoplastic pH.

To test whether and how auxin changes the activity of PM H<sup>+</sup>-ATPases in roots, we performed an ATP hydrolysis assay measuring the hydrolytic release of inorganic phosphate from the ATP, which has been shown to correlate with the activity of the H<sup>+</sup>-ATPases and with the H<sup>+</sup>-extrusion<sup>21,22</sup>. After 1 hour 100 nM IAA treatment, we detected increased ATP hydrolysis activity in root protein extracts (Fig. 2b), similarly as observed in shoots following auxin treatment (Lin et al., submitted). This supports the notion that auxin activates H<sup>+</sup>-pumps also in root cells, which should lead to apoplast acidification contrasting with the observed alkalisation (see Fig. 1b).

Hereafter, we reanalysed the phospho-proteomics data specifically for the phosphorylation of Thr<sup>947</sup> in AHA2, a known activation site<sup>23,24</sup>. Thr<sup>947</sup> was significantly more phosphorylated after IAA treatment (Fig. 2c), suggesting that auxin activates AHAs in the root by stimulating this phosphorylation. To confirm the phosphorylation state of AHA2, we used antibodies that specifically recognize the catalytic domain of AHA2 and phosphorylated Thr<sup>947</sup>. We pre-treated seedlings with 50  $\mu$ M of the auxin biosynthesis inhibitor kynurenine for 24 hours, followed by 10 nM IAA treatment and harvested roots at given time points. At such low concentration, IAA strongly induced phosphorylation of Thr<sup>947</sup> of AHA2 within 10-20 minutes and additionally led to an increase of AHA2 protein levels at later time points (Fig. 2d). Thus, auxin mediates AHA2 phosphorylation leading to its activation.

Our results show that, consistently with previous findings in shoots<sup>7,22</sup>, auxin rapidly induces AHA phosphorylation leading to H<sup>+</sup>-pump activation in the root. This, however, should lead to apoplast acidification and not the observed auxin-induced apoplast alkalisation (see Fig. 1b) suggesting that in

roots H<sup>+</sup>-pump activation may act antagonistically, presumably as a negative feed-back to auxin-mediated apoplast alkalisation.

### **H<sup>+</sup>-ATPases activation counteracts auxin-mediated apoplast alkalisation and growth inhibition**

To better understand the role of H<sup>+</sup>-pump activation during auxin-mediated root growth inhibition, we used the fungal toxin Fusicoccin (FC). FC stabilizes binding of 14-3-3 proteins to H<sup>+</sup>-ATPases, thus rapidly and specifically activating them<sup>23,25,26</sup>, without otherwise affecting auxin signalling (Extended Data Fig. 2a). This allowed us to dissect the effects of auxin and H<sup>+</sup>-ATPase activation on pH and growth simultaneously. FC caused rapid apoplast acidification and promoted growth in roots (Extended Data Fig. 2b, c), opposite to the auxin effect. When FC and IAA were applied simultaneously, we observed an intermediate outcome on apoplastic pH and root growth proportional to the ratio of auxin versus FC (Fig. 2e, f and Extended Data Fig. 2f, g). Similar observations were made when FC and IAA were added sequentially (Extended Data Fig. 2b-e). These observations suggest that FC-mediated H<sup>+</sup>-ATPase activation and IAA-mediated apoplast alkalisation act antagonistically during apoplastic pH and root growth regulation.

To test this notion genetically, we analysed auxin response of loss- and gain-of-function *aha* mutants. Single *aha1* and *aha2* mutants have no consistent root phenotypic defects, when grown on auxin (Extended Data Fig. 2h), while the double mutant is embryo-lethal<sup>27</sup>. To overcome redundancy within the AHA family and test for AHA function specifically in cells where root growth is controlled, we used a synthetic trans-acting siRNA<sup>28</sup> targeting *AHA1/2/7/11* (*AtTAS1c-AHA*), expressed from the *PIN2* promoter in the outer root tissues<sup>29</sup>. Expression of all four AHAs was verifiably downregulated in both independent transgenic lines (Extended Data Fig. 2i). Both *AtTAS1c-AHA* lines were hypersensitive to auxin in terms of apoplast alkalisation (Fig. 2g) and root growth inhibition (Fig. 2i). In contrast, constitutive activation of AHA1 in the *ost2-3D* mutants<sup>30</sup> resulted in decreased auxin sensitivity of apoplastic pH (Fig. 2h) and root growth (Fig. 2i). These *aha* mutant phenotypes further confirm that auxin-mediated H<sup>+</sup>-ATPase activation antagonizes auxin-induced apoplast alkalisation in the root.

These observations show that H<sup>+</sup>-pump activation in roots acts against the observed auxin-mediated apoplast alkalisation. The auxin effect on root growth is thus the net result of auxin-induced AHA activation, which presumably acts as negative feed-back against the more dominant auxin-mediated alkalisation.

### **TMK1 interacts with H<sup>+</sup>-ATPases**

To gain insights into the mechanisms, by which auxin signalling regulates apoplastic pH, we performed co-immunoprecipitation pull-down assays followed by MS-assisted identification of proteins associated with either the intracellular TIR1/AFB1 receptor or the cell surface TMK1 Leucine-rich repeat receptor-like

kinase<sup>31</sup>. For TIR1 and AFB1 this approach did not reveal any components that have yet been linked to control of H<sup>+</sup>-transport (Extended Data Fig. 3a and Extended Data Table 2). For TMK1, although enrichment was not strong and the identified peptides did not allow discriminating between the two proteins, we found peptides of AHA1/AHA2 among the top enriched associated peptides for TMK1 (Extended Data Fig. 3b and Extended Data Table 3).

To verify the interaction between AHAs and TMK1, we performed Co-IP assays from transgenic *pTMK1::TMK1-FLAG* (Fig. 3a), *pAHA2::AHA2-GFP* (Fig. 3b) and *pTMK1-TMK1-GFP* roots (Extended Data Fig. 3c). In all pulldowns with TMK1-expressing plants, we detected associated AHA2 and reciprocally from the AHA2-GFP pulldowns, we detected TMK1, confirming interaction between TMK1 and AHA2. IAA treatment had no effect on the interaction, but AHA2 phosphorylation was increased (Fig. 3a, b and Extended Data Fig. 3c). Additionally, we confirmed the interaction *in vivo* by bimolecular fluorescent complementation (BiFC) in tobacco leaves co-transformed with TMK1 and AHA2 (Fig. 3c and Extended Data Fig. 3d).

These observations show that TMK1, a presumable component of cell surface auxin signalling, interacts with the PM H<sup>+</sup>-ATPase AHA2.

### **TMK1 activity mediates auxin effect on H<sup>+</sup>-ATPases phosphorylation and activation**

To test the role of TMK1 in H<sup>+</sup>-ATPase phosphorylation, we performed phospho-proteomic analysis in roots of *tmk1-1* compared to WT, and detected strong hypophosphorylation of AHAs in the *tmk1-1* (Fig. 3d and Extended Data Table 1). This stipulates that TMK1 is involved in H<sup>+</sup>-ATPases phosphorylation.

To further confirm this notion, we cloned *p35S::TMK1-HA* and two kinase-dead versions with mutations in the ATP binding site, in which K<sup>616</sup> is exchanged to either E or R (TMK1<sup>K616E</sup> or TMK1<sup>K616R</sup>). Transient overexpression of the wild type (WT), but not the kinase-dead TMK1 constructs in tobacco resulted in rapid wilting of the leaves (Extended Data Fig. 3e), an effect consistent with PM H<sup>+</sup>-ATPases activation<sup>32</sup>. To test this directly in *Arabidopsis* roots, we generated dexamethasone (DEX)-inducible TMK1 gain-of-function lines and assessed the phosphorylation status of AHA2. In the root extract expressing TMK1<sup>K616R</sup>, no phosphorylation of AHA<sup>Thr947</sup> was observed after 100 nM IAA treatment compared to TMK1<sup>WT</sup> (Extended Data Fig. 3f).

Next, we analysed different *tmk* loss-of-function mutants. We detected less auxin-induced AHA phosphorylation in *tmk1-1* single and *tmk1-1, tmk3-1* (*tmk1,3*) double mutants compared to WT (Fig. 3e, f and Extended Data Fig. 3g, h). As double *tmk1-1, tmk4-1* (*tmk1,4*) plants were very stunted, protein extracts were prepared from full seedlings and less endogenously phosphorylated AHA2 was detected (Fig. 3g). We also assessed the H<sup>+</sup>-ATPase activity by the ATP hydrolysis assay. We detected auxin-induced increase of H<sup>+</sup>-ATPase activity in WT but not in the *tmk1-1*, *tmk4-1* and *tmk1,4* roots (Fig. 3h).

In summary, these independent approaches show that active TMK1 kinase is required for the auxin-mediated phosphorylation and activation of H<sup>+</sup>-ATPases in roots.

### **TIR1/AFB and TMK1 signalling converge antagonistically on apoplastic pH and growth regulation**

Our results show that TMK1 interacts with, and mediates the phosphorylation and activation of PM H<sup>+</sup>-ATPases (see Fig. 3), which results in apoplast acidification (see Fig. 2). How can we reconcile this with the observed auxin-mediated apoplast alkalinisation leading to growth inhibition (see Fig. 1)?

Previously, it was proposed that the auxin influx transporter AUXIN RESISTANT1 (AUX1) and the intracellular TIR1/AFB auxin receptors mediate auxin-induced membrane depolarisation associated with changes in H<sup>+</sup>-fluxes across the PM<sup>15,33</sup>. Therefore, we set out to assess the interplay of these components with TMK1 action in regulation of apoplastic pH. First, we used *aux1-100* mutants defective in the AUXIN RESISTANT 1 (AUX1), which mediates cellular uptake of IAA and, in particular, of the synthetic auxin analogue 2,4-dichlorophenoxyacetic acid (2,4-D)<sup>34</sup>. Consistently with previous reports<sup>9</sup>, *aux1-100* roots were less sensitive to 5 nM IAA in the vRootchip (Extended Data Fig. 4a, b) or to 0.1 μM 2,4-D (Extended Data Fig. 4c, d) in the steady-state conditions, both for the apoplastic pH and the root growth inhibition suggesting intracellular auxin perception is required for auxin-mediated apoplast alkalinisation.

Given that intracellular TIR1/AFB receptors mediate auxin-mediated growth inhibition<sup>9</sup>, we evaluated apoplastic pH in parallel to growth in the *tir1-1*, *afb2-1*, *afb3-1* (*tir triple*) mutant. The *tir triple* roots were resistant to 5 nM IAA in both apoplast alkalinisation and growth inhibition (Fig. 4a and Extended Data Fig. 4e). As a pharmacological alternative, we applied PEO-IAA, which acts as an anti-auxin and blocks downstream signalling following binding to TIR1/AFB receptors<sup>35</sup>. Simultaneous addition of 10 μM PEO-IAA and 5 nM IAA prevented apoplast alkalinisation and growth inhibition (Extended Data Fig. 4f, g). Both approaches further corroborate the involvement of the TIR1/AFB auxin perception in auxin-mediated apoplast alkalinisation.

To test the TIR1/AFB requirement, definitively, we took advantage of the cvxIAA/ccvTIR1 system, in which the engineered concave (ccv) TIR1 receptor cannot interact with the natural IAA, but only with a synthetic convex (cvx) IAA analogue, thus allowing specific activation of TIR1/AFB signalling<sup>7</sup>. Application of 50 nM cvxIAA in the vRootchip resulted in apoplastic alkalinisation in the ccvTIR1 plants, but not in the control (Fig. 4b), confirming that specific activation of the TIR1/AFB pathway is sufficient to induce root growth inhibition<sup>9</sup> and apoplast alkalinisation.

These observations suggest that intracellular TIR1/AFB signalling mediates the dominant auxin effect: apoplast alkalinisation and root growth inhibition. This is then counteracted by the cell surface TMK1-mediated H<sup>+</sup>-ATPase activation for apoplast acidification. Indeed, in the steady state, TMK1

function is redundantly required for root growth as demonstrated by shorter roots in *tmk* mutants (Fig. 4c)<sup>36</sup>. In response to low concentration of auxin, *tmk1*-related mutants were more sensitive (Fig. 4d), while overexpressing TMK1 (*pUBQ10::TMK1-3HA*) led to a slight auxin resistance (Extended Data Fig. 4h). This resembles the corresponding loss- and gain-of-function *aha* mutants (see Fig. 2) providing additional support for the antagonistic, growth-promoting role of TMK-mediated AHA activity.

To explore further the antagonism of TIR1/AFB and TMK1, we created double mutant *tmk1-1, tir1-1* (*tmk1, tir1*) and analysed the auxin effect on apoplastic pH and root growth. As expected, the *tmk1, tir1* mutant showed intermediate auxin sensitivity compared to the single mutants both for growth and apoplastic pH (Fig. 4e, f and Extended Data Fig. 4i, j).

Collectively, these results strongly suggest that auxin activates two antagonistically acting signalling pathways: (i) the cell surface, TMK1-mediated H<sup>+</sup>-efflux acidifying apoplast and (ii) an intracellular TIR1/AFB-dependent apoplast alkalinisation leading to the rapid growth inhibition (Fig. 4g). It seems that the TIR1/AFB-mediated apoplast alkalinisation is dominant, in particular at conditions of higher auxin after its exogenous application. But at low auxin levels, TMK1-mediated acidification becomes more apparent and fine-tunes the growth inhibition outcome.

## Conclusions

Our findings provide novel insights into a long-standing question on how root growth is regulated in plants. In particular, we address the old mystery of opposite growth regulation in shoots and roots by the phytohormone auxin and we also clarify the downstream cellular mechanism of auxin-mediated root growth inhibition.

Auxin regulates root growth very rapidly, utilizing a non-transcriptional branch of a signalling pathway downstream of intracellular TIR1/AFB receptors<sup>9</sup>. This pathway mediates apoplast alkalinisation, which we show as the direct, causative cellular mechanism for root growth regulation. This finding extends the classical Acid Growth Theory proposing that low apoplastic pH promotes growth<sup>2,3</sup>. We demonstrate validity of this mechanism also for growth inhibition, showing that root growth rate is immediately and reversibly determined by apoplastic pH changes.

Remarkably, the auxin-mediated apoplast alkalinisation in roots does not occur through the regulation of PM H<sup>+</sup>-ATPases as observed in shoots, where the same TIR1/AFB auxin perception mechanism leads to PM H<sup>+</sup>-ATPases activation and apoplast acidification<sup>5,7,22</sup>.

Instead, in roots, PM H<sup>+</sup>-ATPases are phosphorylated and activated via the cell surface TMK1 receptor like kinase-based auxin signalling, which leads to apoplast acidification and root growth promotion. This mechanism, acting antagonistically to the more dominant TIR1/AFB-mediated alkalinisation, constitutes a negative feed-back, presumably to fine-tune root growth to be able to rapidly



respond to subtle changes of environmental stimuli.

Key remaining open questions are: (i) if not by PM H<sup>+</sup>-ATPases, how does TIR1/AFB signalling mediate alkalinisation in roots? A plausible scenario would be a rapid increase in H<sup>+</sup>-permeability across the PM, which may be mediated by TIR1/AFB-activated Ca<sup>2+</sup> signalling<sup>33</sup> and would impact on the apoplastic pH and membrane potential. (ii) What is the auxin perception mechanism for the TMK1 pathway? Is it direct activation of TMK1 by auxin or through another yet to be identified associated auxin receptor?

With cell surface-based TMK1 activating H<sup>+</sup>-pumps and intracellular TIR1/AFB signalling causing the net cellular H<sup>+</sup>-influx, two auxin-triggered antagonistic mechanisms converge on the regulation of extracellular pH, which directly determines root growth rates. This seemingly counterproductive simultaneous ‘gas and brake’ action presumably poises the root tip for rapid and flexible changes of the growth rate and direction in response to numerous stimuli during the challenging task to navigate through the complex soil environments.

## References

- 1 Spartz, A. K. *et al.* SAUR inhibition of PP2C-D phosphatases activates plasma membrane H<sup>+</sup>-ATPases to promote cell expansion in Arabidopsis. *Plant Cell* **26**, 2129-2142 (2014).
- 2 Rayle, D. L. & Cleland, R. Enhancement of wall loosening and elongation by acid solutions. *Plant Phys.* **46**, 250-253 (1970).
- 3 Hager, A., Menzel, H. & Krauss, A. Versuche und hypothese zur primärwirkung des auxins beim streckungswachstum. *Planta* **100**, 47-75 (1971).
- 4 Du, M., Spalding, E. P. & Gray, W. M. Rapid auxin-mediated cell expansion. *Annu. Rev. Plant Biol.* **71**, 379-402 (2020).
- 5 Fendrych, M., Leung, J. & Friml, J. TIR1/AFB-Aux/IAA auxin perception mediates rapid cell wall acidification and growth of Arabidopsis hypocotyls. *Elife* **5**, e19048 (2016).
- 6 Chapman, E. J. & Estelle, M. Mechanism of auxin-regulated gene expression in plants. *Annu. Rev. Genet.* **43**, 265-285 (2009).
- 7 Uchida, N. *et al.* Chemical hijacking of auxin signaling with an engineered auxin–TIR1 pair. *Nat. Chem. Biol.* **14**, 299 (2018).
- 8 Pickett, F. B., Wilson, A. K. & Estelle, M. The *aux1* mutation of Arabidopsis confers both auxin and ethylene resistance. *Plant Phys.* **94**, 1462-1466 (1990).
- 9 Fendrych, M. *et al.* Rapid and reversible root growth inhibition by TIR1 auxin signalling. *Nat. Plants* **4**, 453 (2018).
- 10 Cao, M. *et al.* TMK1-mediated auxin signalling regulates differential growth of the apical hook. *Nature* **568**, 240-243 (2019).
- 11 Chen, X. *et al.* Inhibition of cell expansion by rapid ABP1-mediated auxin effect on microtubules. *Nature* **516**, 90 (2014).
- 12 Adamowski, M., Li, L. & Friml, J. Reorientation of cortical microtubule arrays in the hypocotyl of *Arabidopsis thaliana* is induced by the cell growth process and independent of auxin signaling. *Int. J. Mol. Sci.* **20**, 3337 (2019).
- 13 Scheuring, D. *et al.* Actin-dependent vacuolar occupancy of the cell determines auxin-induced growth repression. *PNAS* **113**, 452-457 (2016).
- 14 Barbez, E., Dünser, K., Gaidora, A., Lendl, T. & Busch, W. Auxin steers root cell expansion via apoplastic pH regulation in *Arabidopsis thaliana*. *PNAS* **114**, E4884-E4893 (2017).
- 15 Monshausen, G. B., Miller, N. D., Murphy, A. S. & Gilroy, S. Dynamics of auxin-dependent Ca<sup>2+</sup> and pH signaling in root growth revealed by integrating high-resolution imaging with automated computer vision-based analysis. *Plant J.* **65**, 309-318 (2011).
- 16 Shih, H.-W., DePew, C. L., Miller, N. D. & Monshausen, G. B. The cyclic nucleotide-gated channel CNGC14 regulates root gravitropism in *Arabidopsis thaliana*. *Curr. Biol.* **25**, 3119-3125 (2015).
- 17 Von Wangenheim, D. *et al.* Live tracking of moving samples in confocal microscopy for vertically grown roots. *Elife* **6**, e26792 (2017).
- 18 Martinière, A. *et al.* Uncovering pH at both sides of the root plasma membrane interface using noninvasive imaging. *PNAS* **115**, 6488-6493 (2018).

- 19 Fuglsang, A. T. *et al.* Receptor kinase-mediated control of primary active proton pumping at the plasma membrane. *Plant J.* **80**, 951-964 (2014).
- 20 Haruta, M., Gray, W. M. & Sussman, M. R. Regulation of the plasma membrane proton pump (H<sup>+</sup>-ATPase) by phosphorylation. *Curr. Opin. Plant Biol.* **28**, 68-75 (2015).
- 21 Kinoshita, T. & Shimazaki, K. i. Blue light activates the plasma membrane H<sup>+</sup>-ATPase by phosphorylation of the C-terminus in stomatal guard cells. *EMBO J.* **18**, 5548-5558 (1999).
- 22 Takahashi, K., Hayashi, K.-i. & Kinoshita, T. Auxin activates the plasma membrane H<sup>+</sup>-ATPase by phosphorylation during hypocotyl elongation in Arabidopsis. *Plant Phys.* **159**, 632-641 (2012).
- 23 Fuglsang, A. T. *et al.* Binding of 14-3-3 protein to the plasma membrane H<sup>+</sup>-ATPase AHA2 involves the three C-terminal residues Tyr<sup>946</sup>-Thr-Val and requires phosphorylation of Thr<sup>947</sup>. *J. Biol. Chem.* **274**, 36774-36780 (1999).
- 24 Svennelid, F. *et al.* Phosphorylation of Thr<sup>948</sup> at the C terminus of the plasma membrane H<sup>+</sup>-ATPase creates a binding site for the regulatory 14-3-3 protein. *Plant Cell* **11**, 2379-2391 (1999).
- 25 Baunsgaard, L., Fuglsang, A. T., Jahn, T., Korthout, H. & Palmgren, M. The 14-3-3 proteins associate with the plant plasma membrane H<sup>+</sup>-ATPase to generate a fusicoccin binding complex and a fusicoccin responsive system. *Plant J.* **13**, 661-671 (1998).
- 26 Olsson, A., Svennelid, F., Ek, B., Sommarin, M. & Larsson, C. A phosphothreonine residue at the C-terminal end of the plasma membrane H<sup>+</sup>-ATPase is protected by fusicoccin-induced 14-3-3 binding. *Plant Phys.* **118**, 551-555 (1998).
- 27 Haruta, M. *et al.* Molecular characterization of mutant Arabidopsis plants with reduced plasma membrane proton pump activity. *J. Biol. Chem.* **285**, 17918-17929 (2010).
- 28 Carbonell, A. *et al.* New generation of artificial microRNA and synthetic trans-acting small interfering RNA vectors for efficient gene silencing in Arabidopsis. *Plant Phys.* **165**, 15-29 (2014).
- 29 Zhang, Y., Xiao, G., Wang, X., Zhang, X. & Friml, J. Evolution of fast root gravitropism in seed plants. *Nat. Commun.* **10**, 1-10 (2019).
- 30 Yamauchi, S. *et al.* The plasma membrane H<sup>+</sup>-ATPase AHA1 plays a major role in stomatal opening in response to blue light. *Plant Phys.* **171**, 2731-2743 (2016).
- 31 Gallei, M., Luschning, C. & Friml, J. Auxin signalling in growth: Schrödinger's cat out of the bag. *Curr. Opin. Plant Biol.* **53**, 43-49 (2020).
- 32 Kinoshita, T. & Shimazaki, K.-I. Analysis of the phosphorylation level in guard-cell plasma membrane H<sup>+</sup>-ATPase in response to fusicoccin. *Plant Cell Physiol.* **42**, 424-432 (2001).
- 33 Dindas, J. *et al.* AUX1-mediated root hair auxin influx governs SCF<sup>TIR1/AFB</sup>-type Ca<sup>2+</sup> signaling. *Nat. Commun.* **9**, 1-10 (2018).
- 34 Yang, Y., Hammes, U. Z., Taylor, C. G., Schachtman, D. P. & Nielsen, E. High-affinity auxin transport by the AUX1 influx carrier protein. *Curr. Biol.* **16**, 1123-1127 (2006).
- 35 Hayashi, K.-i. *et al.* Rational design of an auxin antagonist of the SCF<sup>TIR1</sup> auxin receptor complex. *ACS Chem. Biol.* **7**, 590-598 (2012).
- 36 Dai, N., Wang, W., Patterson, S. E. & Bleeker, A. B. The TMK subfamily of receptor-like kinases in Arabidopsis display an essential role in growth and a reduced sensitivity to auxin. *PLoS One* **8**, e60990 (2013).

## Figure Legends

### Figure 1. Auxin rapidly inhibits root growth by alkalinising the apoplast

**a**, Time lapse of the apoplastic pH response in root tip epidermal cells to 5 nM IAA treatment followed by auxin washout (basal auxin-free medium) in vRootchip. pH was monitored in the same region of interest (ROI) for 36 minutes by the ratiometric HPTS dye. The ratio-image represents the ratio of excitation 488 nm and 405 nm. ROI covers maturation zone (MZ), elongation zone (EZ) and transition zone (TZ). TL is transmitted light image.

**b**, Quantitative analysis of the auxin-induced apoplast alkalinisation in the EZ reported by HPTS dye and corresponding inhibition and recovery of root tip growth rate (GR) following 5 nM IAA and washout as in (a). Means of 4 roots + SD.

**c**, Quantitative analysis of the auxin-induced cytoplasm acidification in the EZ, visualized by the PM-cyto reporter and the corresponding inhibition and recovery of GR upon 5 nM IAA treatment and washout in vRootchip. Means of 3 roots +SD.

**d-g**, Time-lapse of root growth response to a pulse of alkaline (pH 6.15) (d) or acidic medium (pH 5.10) (f). The slope of the white dotted line that tracks the root tip indicates the GR. Quantifications of GR in d (n = 8) (e) and f (n = 7) (g). The shaded areas represent the duration of the indicated treatments. Mean +SD.

### Figure 2. Auxin-triggered H<sup>+</sup>-ATPase phosphorylation and activation counteract auxin-mediated apoplast alkalinisation and growth inhibition

**a**, Representation of the phospho-sites in the model of the *Arabidopsis thaliana* H<sup>+</sup>-ATPase 2 (AHA2) identified in the phospho-proteomic analysis of auxin-treated root samples (2 minutes of 100 nM IAA). The color reflects their impact on the H<sup>+</sup>-translocation activity (green for activation and orange for inhibition).

**b**, Quantification of ATP hydrolysis induction in root samples treated with 100 nM IAA for 1 hour in comparison to mock-treated roots. The IAA-treated sample was normalized by the corresponding mock-treated sample. Bars indicate means of 3 biological replicates + SD. Unpaired t-test. \* p≤0.05.

**c**, Phospho-proteome detection of auxin-induced AHA2-Thr<sup>947</sup> phosphorylation after 2 minutes of 100 nM IAA treatment. n= 4. Box plot depicts minimum to maximum, mean  $\pm$  SD. Two-sample t-test (part of MaxQuant-Perseus analysis). \*\*p $\leq$ 0.01.

**d**, Time-course western blot analysis of auxin-induced Thr<sup>947</sup>-phosphorylated AHA2 levels in roots treated with 10 nM IAA using AHA2 and pThr<sup>947</sup>-specific antibodies. Total AHA2 protein levels were monitored in the same samples as a control. Band intensities of the different lanes are quantified by the Gels Analysis function in ImageJ.

**e-f**, Apoplastic pH (**e**) and root growth (**f**) analysis upon pharmacological activation of H<sup>+</sup>-pumps by 10  $\mu$ M FC and 10 nM IAA in vRootchip. Apoplastic pH was monitored using HPTS. The shaded area represents the duration of the indicated treatment. Mean of 4 roots for each treatment + SD. p $\leq$ 0.0001 between IAA and IAA+FC, from 0 – 32 min (**e**), from 0 – 31 min (**f**), Two-way ANOVA.

**g-h**, Apoplastic pH response in two independent AHA knock-down lines (*AtTAS1c-AHA#2* and #4) (n > 9) (**g**), and the *ost2-3D* gain-of-function allele (n > 5) (**h**) in response to 30 minutes 5 nM IAA treatment. Apoplastic pH changes are determined by the HPTS dye and IAA treatment was normalized to the corresponding mock-treatment. \*\*p $\leq$ 0.01, \*\*\*p $\leq$ 0.001, \*\*\*\*p $\leq$ 0.0001, One-way ANOVA.

**i**, Dose-response of auxin-induced root growth inhibition of *AtTAS1c-AHA* lines and *ost2-3D* mutants reveals hypersensitivity and resistance respectively to IAA in comparison to WT (n > 15) (**i**). The relative GR is calculated by the ratio of GR for each IAA concentration relative to mock-treated GR of the same genotype. \*p $\leq$ 0.05, \*\*p $\leq$ 0.01, \*\*\*p $\leq$ 0.001, \*\*\*\*p $\leq$ 0.0001, Welch ANOVA.

### **Figure 3. TMK1 directly mediates auxin-induced H<sup>+</sup>-ATPase activation.**

**a**, Co-immunoprecipitation (co-IP) of the *pTMK1::TMK1-FLAG* from roots mock or 100 nM IAA-treated for 30 minutes, followed by Western blot detection of AHA2 and Thr<sup>947</sup>-phosphorylated AHA2. The control is the co-IP of WT (Col-0) roots.

**b**, Co-IP of *pAHA2::AHA2-GFP* from roots, followed by Western blot detection of TMK1 and Thr<sup>947</sup>-phosphorylated AHA2 on roots mock or 100 nM IAA-treated for 30 minutes. Interaction does not depend

on auxin presence, but auxin-induced phosphorylation of the interacting AHA2 was observed. As a control sample we include input of *pAHA2::AHA2-GFP* roots.

**c**, Bimolecular Fluorescent Complementation (BiFC) in *Nicotiana benthamiana* leaves transiently transformed either with *TMK1-YFP<sup>N</sup>* (*TMK1* in *pSPYNE*), *YFP<sup>C</sup>-AHA2* (*AHA2* in *pSPYCE*) or both. Scale bar = 10  $\mu$ m.

**d**, Differentially detected phospho-sites of AHAs in *tmk1-1* normalized to WT (Col-0) MS detection levels. We observe less phosphorylation on the indicated phospho-sites in AHA1, AHA2 and AHA3 in the *tmk1-1* mutant. Green indicates the sites with known activation function, while orange is used for known inhibitory function. n= 4. Box plot depicts minimum to maximum, mean  $\pm$  SD. Two-sample t-test (part of MaxQuant-Perseus analysis).

**e**, Western blot analysis of auxin-induced AHA2 Thr<sup>947</sup> phosphorylation in WT and *tmk1-1* roots treated with 100 nM IAA for 1 hour. AHA2 levels were determined as a control.

**f**, Quantification of the auxin effect on AHA2 phosphorylation in (**d**) by normalising the intensity ratio of pThr<sup>947</sup> to AHA2 in auxin-treated root samples to the same ratio in mock-treated samples of the respective genotypes.

**g**, Western blot detection of the AHA2 levels and its Thr<sup>947</sup> phosphorylation in full seedlings shows reduced AHA2 phosphorylation in *tmk1,4* compared to WT.

**h**, Auxin-induced ATP hydrolysis activity is impaired in *tmk* mutants relative to WT roots (1 hour mock or 100 nM IAA treatment). The IAA-treated sample was normalized to the mock-treated WT. Means of 3 biological replicates + SD. \*p $\leq$ 0.05, ns p>0.05, One-way ANOVA.

#### **Figure 4. TIR1/AFB and TMK1 signalling converge antagonistically on apoplastic pH and growth regulation.**

**a**, Apoplastic pH analysis by the HPTS dye shows an impaired auxin response (to 5nM IAA) in *tir triple* mutant roots (in red) compared to WT roots (in black) in vRootchip. Means of 3, 2 roots + SEM. p $\leq$ 0.0001, Two-way ANOVA.

**b**, Apoplastic pH analysis by the HPTS dye shows apoplastic alkalinisation in *ccvTIR1* line (in red) compared to the *control* line (in black) in response to cvxIAA in vRootchip. Means of 2, 3 roots + SEM.  $p \leq 0.01$ , from 0 - 5 minutes, Two-way ANOVA. The shaded area represents the duration of the indicated treatment.

**c**, Steady-state root growth over 6 hours in *tmk1*-related mutants.  $n = 6$  for *tmk1,4*;  $n > 26$  for others. \*\*\*\* $p \leq 0.0001$ , One-way ANOVA.

**d**, Dose-response of auxin-induced root growth inhibition of *tmk1*-related mutants relative to WT and a complemental line (*pTMK1::TMK1-FLAG* in *tmk1-1*). Relative GR is the ratio between auxin-affected growth and mock growth for the same genotype.  $n > 15$ . \* $p \leq 0.05$ , \*\* $p \leq 0.01$ , \*\*\* $p \leq 0.001$ , \*\*\*\* $p \leq 0.0001$ , Welch ANOVA.

**e-f**, Apoplastic pH (**e**) and root growth (**f**) measurement in *tmk1-1*, *tir1-1* and *tmk1-1,tir1-1* mutants in response to 5 nM IAA. The apoplastic pH is indicated by the HPTS emission ratio after 50 minutes treatment. The root growth is measured after 6 hours.  $n > 16$  for both graphs, ns  $p > 0.05$ , \*\* $p \leq 0.01$ , \*\*\* $p \leq 0.001$ , \*\*\*\* $p \leq 0.0001$ , one-way ANOVA.

**g**, Model for auxin-mediated root growth regulation. Auxin induces rapid  $H^+$ -influx across the PM to alkalinise the apoplast and inhibit root growth through an intracellular, non-transcriptional branch of the TIR1/AFB signalling pathway. Concomitantly, auxin through cell surface TMK1 activates  $H^+$ -pumps (AHAs) to promote  $H^+$ -efflux to acidify apoplast and promote growth.

## Methods

### Plant materials and growth conditions

All *Arabidopsis thaliana* mutants and transgenic lines used are in Columbia-0 (Col-0) background. The *pEB1b::EB1b-GFP*<sup>1</sup>, *p35S::MAP4-GFP*<sup>2</sup>, *pSYP22::SYP22-YFP*<sup>3</sup>, *DR5::LUC*<sup>4</sup>, *PM-cyto*<sup>5</sup> marker lines were described previously. The *tir1-1/afb2-1/afb3-1* mutant<sup>6</sup>, *pTIR1::ccvTIR1* in *tir1-1/afb2-3*<sup>7</sup>, *pTIR1::TIR1* in *tir1-1/afb2-3* (we called it control for ccvTIR1)<sup>7</sup> and *aux1-100*<sup>8,9</sup> were donated by the authors. The *pTIR1::TIR1-VENUS* in *tir1-1*<sup>10</sup>, *pAFB1::AFB1-VENUS* in *afb1-3*<sup>11</sup> are shared by Stefan Kepinski. The *aha* mutants are the following: *aha2-5* (SALK\_022010), *aha1-7* (SALK\_065288)<sup>12</sup>, *ost2-3D* shared by Atsushi Takemiya<sup>13</sup>. Two independent lines *AtTAS1c-AHA*#2 and #4 were generated by Jian Chen and Steffen Vanneste as follows: the syn-tasiRNA target sequence was inserted into *pENTR-AtTAS1c-B/c*<sup>14</sup> using hybridized primers TAS-AHA pair (Extended Data Table 4) and was recombined into *pH7m24GW*<sup>15</sup> together with *pDONR P4-P1R* carrying the *pPIN2* promoter<sup>16</sup>, to generate *pPIN2:AtTAS1c-AHA*. The *pAHA2::AHA2-GFP* seeds were donated by Anja T. Fuglsang<sup>17</sup>. The *tmk* mutants are the following: *tmk1-1* (SALK\_016360)<sup>18</sup>, *tmk4-1* (GABI\_348E01)<sup>19</sup> ordered from NASC; Tongda Xu kindly contributed *tmk1-2* (SAIL\_812\_G09), *tmk1-3* (SALK\_008771)<sup>20</sup>, the complemented *pTMK1::gTMK1-FLAG* in *tmk1-1*<sup>20</sup> and *tmk1-1/tmk4-1* double mutant seeds. The transgenic plant lines carrying *DEX::TMK1-HA* and *DEX-TMK1-HA K616R* were generated by Hong Ren and William M. Gray. The *DEX::TMK1* (or *TMK1-K616R/E*)-*HA* constructs were done by cloning the cDNA of *TMK1* (or *TMK1-K616R/E*) without stop codon (Extended Data Table 4) into *pENTR/D-TOPO*, and subsequently recombining into the *pBAV154*<sup>21</sup> binary vector used Gateway system. The *pUBQ10::gTMK1-3HA* and *35S::gTMK1-eGFP* lines were generated by amplifying *TMK1* full length gDNA without stop codon from Col-0 genomic DNA using the primers indicated in Extended Data Table 4. *TMK1* gDNA was inserted into *pDONR221*, subsequently recombined into *pB7m34GW* together with *pDONR P4-P1R* carrying the *pUBQ10* promoter or *TMK1* promoter and *pDONR P2R-P3 3xHA* or *pDONR P2R-P3 eGFP*, respectively. The constructs were transformed into the *Agrobacterium tumefaciens* strain pGV3101 by electroporation and further into Col-0 plants by floral dip.

Seeds were surface-sterilized by chlorine gas, sown on half-strength Murashige and Skoog (½ MS) medium supplemented with 1% (w/v) sucrose and 0.8% (w/v) phyto agar (pH 5.9), stratified in the dark at 4°C for 2 days and then grown vertically at 21°C with a long-day photoperiod (16h light/8h dark). Light sources used were Philips GreenPower LED production modules [in deep red (660 nm)/far red (720 nm)/blue (455 nm) combination, Philips], with a photon density of 140.4  $\mu\text{mol}/\text{m}^2/\text{s} \pm 3\%$ .

## **Microfluidics**

The microfluidic vRootchip was used to analyze root tip growth and apoplastic pH in real-time. The manufacturing of the chip, sample preparation procedure and data analysis of root tip growth were performed as described previously<sup>22</sup>. Our new design contains an additional valve in the control layer that closes the ends of the root channels (Extended Data Fig. 1m). In case of air bubbles in the root channels, the additional valve allows pressurizing the channel and air will be absorbed into the Polydimethylsiloxane (PDMS) chip material within 2-10 minutes. Afterwards, experiments started after adaptation of at least two hours. Besides, we introduced a graphical user interface (Extended Data Script 1) using the Processing software (<https://processing.org/>) with the ControlIP5 package (<http://www.sojamo.de/libraries/controlIP5/>) that sends serial commands to the Arduino. A sketch (Extended Data Script 2) runs on the Arduino to operate the electronics and receive commands. For one vRootchip, maximum 8 samples were used. When comparing two genotypes, 3-4 seedlings were used for each genotype and mounted in alternating channels to minimize the time difference between imaging the two genotypes. For each root, we imaged one ROI containing early elongating epidermal cells and the other ROI covering the root tip. As these two ROIs were captured sequentially, we imaged the apoplastic pH and the growth of the same root close to simultaneously.

## **Scanner growth assay**

To complement the real-time imaging in the vRootchip, growth analysis was performed on a vertical scanner with bigger sample sizes allowing more conditions to be evaluated. This growth measurement we



called steady-state. 4-day-old seedlings were transferred to 60 × 15 mm petri dishes filled with 5 ml of ½ MS medium with treatments as indicated. The petri dishes were placed on a vertically mounted flatbed scanner (Epson perfection V370) and seedlings were imaged through the layer of medium. Either wet black filter paper or ½ MS medium containing activated charcoal was placed in the lid of the petri dishes to improve background contrast. The samples were automatically imaged every 10 or 30 minutes using the AutoIt script described previously<sup>23</sup> and scans were taken at 1200 dpi. The resulting image series were analyzed using StackReg stabilization and the Manual Tracking plugin in ImageJ.

### **Imaging and measuring apoplastic pH with HPTS dye**

pH measurements were done both in steady-state condition and real-time vRootchip imaging. For steady-state pH analysis, 4-day-old seedlings were transferred to ½ MS medium containing 1 mM HPTS (Thermo Scientific 6358-69-6, dissolved in ddH<sub>2</sub>O) and indicated treatments for 30 or 50 minutes as indicated. Subsequently, seedlings on a slice of the treatment medium were mounted into a Lab-Tek Chambered Coverglass for steady state imaging. Real-time imaging of the apoplastic pH was done in vRootchip containing medium (¼ MS + 0.1% sucrose) supplemented with 1mM HPTS with or without treatment. All imaging was performed on the in-house established vertical Zeiss LSM 800 confocal microscope<sup>24</sup>. Fluorescent signals for protonated HPTS (excitation 405 nm, emission 514 nm, visualized in red) and deprotonated HPTS (excitation, 488 nm, emission 514 nm, visualized in green) were detected with a 20x/0.8 air objective. Image analysis was performed on a cropped region of elongating epidermis cells using a batch processing modification of a previously described the ImageJ macro<sup>25</sup>. The relative pH value is calculated as the background-subtracted intensity of the deprotonated intensity divided by that of the protonated intensity to represent the relative pH. The resulting relative pH data were plotted over time and statistically evaluated in GraphPad Prism 6. Note that we did not transform the relative pH value to the absolute pH values, which would require the generation of a calibration curve for each experiment.

### **Imaging and measuring cytosolic pH with the *PM-cyto* reporter line**

Real-time imaging of the cytosolic pH near the PM was done by using the *PM-cytp* reporter line in vRootchip containing medium ( $\frac{1}{4}$  MS + 0.1% sucrose), and was imaged on the in-house established vertical Zeiss LSM 800 confocal microscope<sup>24</sup>. Sequential illumination at 488 and 405 nm with emission 514 nm for both, corresponding to the two absorption peaks of pHluorin, were taken with a 20x/0.8 air objective. For each root in the vRootchip, two ROI with one containing the elongating epidermal cell for measuring the cytosolic pH and one containing the root tip for measuring the root growth rate were tracked over time. Image analysis was performed similar to the HPTS analysis described above.

### **Imaging microtubule orientation and vacuolar morphology**

The *pEB1b::EB1b-GFP* marker line was used to track the dynamics of CMT orientation in vRootchip. Images were obtained every 6.25 s and the analysis of the CMT orientation was done in ImageJ by max Z-projection on every 10 frames and quantification by a for batch processing modified version of the Fibril Tool macro<sup>26</sup>. The *p35S::MAP4-GFP* marker line was used for capturing the CMT orientation after treatment for the indicated time period. The CMT orientation angle was processed using the Bioline script<sup>27</sup>. For both marker lines, the GFP (excitation 488 nm, emission 514 nm) signal was detected by Plan-Apochromat 20x/0.8 air objective in the vertical Zeiss LSM 800 confocal microscope<sup>24</sup>.

The *pSYP22::SYP22-YFP* marker line was used for imaging vacuolar morphology. We used a mounting system<sup>28</sup>, which allows the injection of new liquid medium during imaging. Images were taken before and 30 minutes after Mock or 100 nM IAA treatment in liquid medium and the YFP (excitation 488 nm, emission 527 nm) intensity was detected with C-Apochromat 40x/1.20 W Korr objective in an inverted Zeiss LSM 800 confocal microscope.

### **Non-invasive microelectrode (MIFE) ion flux measurements**

Net H<sup>+</sup> flux was measured using non-invasive microelectrode ion flux estimation (MIFE) technique essentially as described elsewhere<sup>29</sup>. Roots of intact 6-day-old *Arabidopsis* WT seedlings were immobilised in a measuring chamber using Perspex holders. The composition of the solution was 0.5 mM KCl and 0.1

mM CaCl<sub>2</sub>; pH 5.8, unbuffered. After 30-40 minutes of conditioning, the H<sup>+</sup> microelectrode was positioned 20 µm from the root surface in the elongation zone (~450 µm from the tip) (from which ion fluxes were measured). Steady-state H<sup>+</sup> fluxes were recorded for 5-10 minutes, and then 10 nM auxin treatment was applied following by another 30-40 minutes of recording. At least 9 individual plants from several batches were used. The sign convention is “influx positive”.

#### **Evaluating the TIR1-transcriptional response using DR5::LUC**

4-day-old DR5::LUC seedlings are placed on the surface of solidified ½ MS medium with 200 µl of 5 mM D-luciferin dissolved in 1x PBS drop on the root tips for 30 minutes as pre-treatment. Subsequently, the samples were transferred to the solidified ½ MS medium supplemented with mock, 10 nM IAA, 10 µM FC and IAA+FC, and immediately imaged in an in-house established dark box with a Photometric Evolve® EMCCD camera equipped with a 17 mm fixed lens/0.95 and an additional 125 mm lens<sup>23</sup>. The multiplier EMCCD gain was set to 70 and the exposure time to 35 sec, and images were acquired every 2 min. The resulting time-lapse video was analysed in ImageJ as described previously<sup>23</sup>.

#### **Identification of TMK1-interacting proteins using IP/MS-MS**

Immunoprecipitation (IP) experiments were performed in three biological replicates as described previously<sup>30</sup> using 1 g of roots of 7-day-old seedlings from the *p35S::TMK1-eGFP* transgenic line and 1 g of roots from WT. Interacting proteins were isolated by incubating total protein extracts with 100 µL anti-GFP coupled magnetic beads (Miltenyi Biotech). Three replicates of *p35S::TMK1-eGFP* were compared to three WT replicates. Tandem mass spectrometry (MS) on a Q-Exactive device (Thermo Fisher) and statistical analysis using MaxQuant and Perseus software was performed as described previously<sup>31</sup>.

#### **Identification of TIR1- and AFB1-interacting proteins using IP/MS-MS**

For immunoprecipitation, ground plant material of *pTIR1::TIR1-VENUS* in *tir1-1* and *pAFB1::AFB1-VENUS* in *afb1-3* transgenic lines was lysed in mild lysis buffer (50 mM Tris pH 7.5, 150 mM NaCl, 2 mM

MgCl<sub>2</sub>, 0.2 mM EDTA, 1xCP1, 0.5 mM DTT, 0.2% NP40 and 1 mg/ml DNase) and mildly sonicated using a Bioruptor (Diagenode). After lysate clearance, supernatant was submitted to enrichment using GFP-Trap agarose beads (Chromotek) for 45 minutes at 4°C while gently rotating. Beads were subsequently washed twice in lysis buffer, twice in detergent-free lysis buffer and three times in 50 mM Ammonium bicarbonate (ABC) (Sigma) with intermediate centrifuging for 2 minutes at 2000g at 4°C. After a final wash, bead-precipitated proteins were alkylated using 50 mM Acrylamide (Sigma). Precipitated proteins were submitted to on-bead trypsin digestion using 0.35 µg trypsin (Roche) per reaction. After overnight incubation at 25°C peptides were desalted and concentrated using C18 StageTips.

After StageTip processing, peptides were applied to online nanoLC-MS/MS using a 60 minutes acetonitrile gradient from 8-50%. Spectra were recorded on a LTQ-XL mass spectrometer (Thermo Scientific) according to<sup>31</sup>. Statistical analysis using MaxQuant and Perseus software was performed as described previously<sup>31</sup>.

### **Phospho-proteomics of auxin-treated roots**

Roots from 5-day-old plants were treated and immediately harvested and flash frozen in liquid nitrogen. They then were ground to fine powder in liquid nitrogen. Powder was suspended in SDS lysis buffer (100 mM Tris pH8.0, 4% SDS and 10 mM DTT) and sonicated using a cooled Bioruptor (Diagenode) for 10 minutes using high power with 30 seconds on 30 seconds off cycle. Lysate was cleared by centrifugation at maximum speed for 30 minutes. Protein concentrations were determined using the Bradford reagent (Bio-Rad).

For FASP 30 kDa cut-off Amicon filter units (Merck Millipore) were used. Filters were first tested by applying 50 µl urea buffer UT buffer (8 M Urea and 100 mM Tris pH8.5) and centrifuging for 10 minutes at 11000 rpm at 20°C. The desired amount of protein sample was next mixed with UT buffer until a volume of 200 µl, applied to filter and centrifuged for 15 minutes. All centrifuge steps were at 11000 rpm at 20°C. Filter was washed with UT buffer for 15 minutes. Retained proteins were alkylated with 50 mM acrylamide (Sigma) in UT buffer for 30 minutes at 20°C while gently shaking followed by a triple wash step with UT

buffer for 15 minutes and three washes with 50 mM ABC buffer. After last wash proteins were cleaved by adding trypsin (Roche) in a 1:100 trypsin:protein ratio. Digestion was completed overnight. The following day filter was changed to a new tube and peptides were eluted by centrifuging for 15 minutes. Further elution was completed by adding two times 50 mM ABC buffer and centrifuging for 10 minutes on 11000 rpm at 20°C.

For peptide desalting and concentrating 200 µl tips were fitted with 2 plugs of C18 octadecyl 47 mm Disks 2215 (Empore™) material and 1 mg:10 µg of LiChroprep® RP-18 : peptides (Merck). Tips were sequentially equilibrated with 100% methanol, 80% ACN in 0.1% formic acid and twice with 0.1% formic acid for 4 minutes at 1500g. After equilibration peptides were loaded for 20 minutes at 400g. Bound peptides were washed with 0.1% formic acid and eluted with 80% ACN in 0.1% formic acid for 4 minutes at 1500g. Eluted peptides were subsequently concentrated using a vacuum concentrator for 30 minutes at 45°C and resuspended in 50 µl of 0.1% formic acid.

For phosphopeptide enrichment magnetic Ti<sup>4+</sup>-IMAC (MagResyn) were used according to manufactures protocol. Enrichments were performed with 1 mg of peptides in biological quadruplicate.

After Stagetip processing, peptides were applied to online nanoLC-MS/MS using a 120 minutes acetonitrile gradient from 8-50% for phospho-proteomics. Spectra recording and statistical analysis were as previously described, with the addition of phosphorylation as a variable modification<sup>31</sup>. Filtering of datasets was done in Perseus in as described<sup>32</sup>.

### **Phospho-proteomics in WT and *tmk1-1* roots**

4 biological samples of Col-0 WT and *tmk1-1* roots were prepared and treated as indicated above. They were submitted to the phospho-proteomic pipeline<sup>31,32</sup> and differentially phosphorylated peptides belonging to H<sup>+</sup>-ATPases were specifically filtered out of the big dataset (Extended Data Table 1).

### **Protein extraction and Western blot analysis for co-IP and determination of AHA2 phosphorylation state**

To isolate PM H<sup>+</sup>-ATPases and potential interactors, 5-7 day-old plant roots were harvested at the indicated time points after 10 or 100 nM IAA auxin treatment. 24 hour prior to the evaluation of auxin effects, these seedlings were sprayed with ½ AM solution containing 30 µM kynurenine. The root samples were flash frozen in liquid nitrogen and ground (Retsch mill, 2x 1 minute at 20 Hz). The root powder was then resuspended in a 1:1 (w/v) ratio in protein extraction buffer (25 mM Tris-HCl, pH 7.5, 150 mM NaCl, 1% Triton X-100, 1x Roche cOmplete™ Protease Inhibitor Cocktail, 1x Roche PhosSTOP™, 1 mM EDTA, 1 mM DTT and 0.5 mM PMSF). The samples were incubated on ice for 30 minutes, followed by a centrifuging step at 10,000g to discard the plant debris. The cleared supernatant containing the proteins of interest was collected and the total protein content was determined using Quick Start Bradford reagent (Bio-Rad). This could further be used for co-immunoprecipitation analysis or for SDS-PAGE analysis. In order not to lose relevant proteins, protein samples were not boiled in the presence of reducing Laemmli buffer and no harsher PM extraction or membrane enrichment was attempted.

For co-immunoprecipitation, root extracts (obtained by extraction in the Lysis buffer supplied in the Miltenyi µMACs kit, supplemented with 1x Roche cOmplete™ Protease Inhibitor Cocktail, 1 mM DTT and 0.5 mM PMSF), were incubated with magnetic beads from the Miltenyi anti-GFP, anti-HA or anti-FLAG µMACs kits (depending on the tags of the proteins of interest) and kept rotating for 4 hour at 4°C. Elution was performed with room-temperature denaturing elution buffer and the proteins were analyzed by SDS-PAGE and Western blot.

Following separation of proteins by SDS-PAGE in a 10% acrylamide gel (Protean® TGX™, Bio-Rad), proteins were transferred to PVDF membranes by electroblotting (Trans-blot® Turbo™, Bio-Rad). The membranes were then incubated in blocking buffer (0.05% Tween-20, 5% milk powder or 3% BSA, 20 mM Tris-HCl, pH 7.5 and 150 mM NaCl) for at least 60 minutes and incubated with antibody solution against the protein of interest.

## **Antibodies**

The anti-AHA2 and anti-Thr<sup>947</sup> AHA2 antibody were shared by Toshinori Kinoshita and used as described previously<sup>33</sup> at final dilution of 1:5000 in TBST buffer + 3% BSA, followed by anti-rabbit IgG secondary antibody conjugated to horseradish peroxidase (HRP) (GE Healthcare, NA934) at a dilution of 1:10000 and chemiluminescence reaction (SuperSignal West Femto, Thermo Scientific). To allow multiple antibody detections using the same PVDF membrane, mild stripping was performed using 15 g/L glycine, 1 g/L SDS, 10 mL/L Tween-20 buffer at pH 2.2 for 2-5 minutes.

### **ATP hydrolysis in root samples**

To deplete endogenous auxin levels in the seedlings, 14-day-old plants were pre-treated with 30  $\mu$ M kynurenine for 24 hour in the dark. Then, the pretreated seedlings were incubated in the presence and the absence of 100 nM indole-3-acetic acid for 60 minutes under dark condition. The roots excised from the seedlings were homogenized in the homogenization buffer (50 mM MOPS-KOH [pH 7.0], 100 mM KNO<sub>3</sub>, 2 mM sodium molybdate, 0.1 mM NaF, 2 mM EGTA, 1 mM PMSF and 20  $\mu$ M leupeptin) and the homogenates were centrifuged at 10,000 g for 10 minutes; the obtained supernatant was further ultra-centrifuged at 45,000 rpm for 60 minutes. The resultant precipitate (microsomal fraction) was resuspended in the homogenization buffer. ATP hydrolytic activity in the microsomal fraction was measured by the release of inorganic phosphate from ATP in a vanadate-sensitive manner following the method published<sup>34</sup> with the following modifications. The microsomal fraction (22.5  $\mu$ L, 0.2 mg/mL) was mixed with the equal volume of the reaction buffer (60 mM MES-Tris [pH 6.5], 6 mM MgSO<sub>4</sub>, 200 mM KNO<sub>3</sub>, 1 mM ammonium molybdate, 10  $\mu$ g/mL oligomycin, 2 mM NaN<sub>3</sub>, 0.1% Triton X-100, 1 mM PMSF and 20  $\mu$ M leupeptin) with or without 1  $\mu$ L of 10 mM sodium orthovanadate. The reaction was started by adding 5  $\mu$ L of 2 mM ATP and terminated by adding 50  $\mu$ L of the stop solution (2.6% [w/v] SDS, 0.5% [w/v] sodium molybdate and 0.6 N H<sub>2</sub>SO<sub>4</sub>) after incubating at 30°C for 30 minutes.

### **Bimolecular Fluorescence Complementation (BiFC)**

Following the method described<sup>35</sup>, the full-length coding sequences of AHA2 and TMK1 without stop codons were amplified by PCR (primers in Extended Data Table 4), cloned into *pENTR/D-TOPO* or *pDONR207* and recombined in *pSPYNE* and *pSPYCE*<sup>36</sup> to generate BiFC expression constructs. The resulting binary vectors were introduced in *Agrobacterium* GV3101 by electroporation and these were cultured until OD<sub>600</sub> 0.8. Syringe infiltration was performed in *Nicotiana benthamiana* leaves as described in<sup>37</sup>. For the constructs of interest, final OD<sub>600</sub> of 0.2 was used and p19 was co-infiltrated at OD<sub>600</sub> 0.1 to avoid gene silencing. Infiltration buffer of pH5.8 contained: 10 mM MgSO<sub>4</sub>, 10 mM MES-KOH and 0.15 mM acetosyringone. TMK1 overexpression, even transiently, has a strong effect on the viability of the leaves, so samples were taken daily after infiltration to determine the optimal balance between expression level and viable leaf cells. To visualize protein interactions, sections of the leaves were imaged using a Zeiss LSM 700 confocal microscope.

#### **Quantitative RT-PCR**

RNA was extracted from 5-day-old light-grown root tips with the RNAeasy Plant Mini Kit (Qiagen), with three biological replicates for each genotype. Two µg of RNA was used for cDNA synthesis (Qiagen). Samples were pipetted in three technical replicates using an automated JANUS Workstation (PerkinElmer) and measured by the Real-time PCR Roche LightCycler 480 using Luna® Universal qPCR mastermix (NEB, M3003S). Primers utilized for assessing gene expression are listed in Extended Table 4. Expression levels were normalized to Elongation factor 1-alpha (At5G60390)<sup>37</sup>.

#### **Statistical analysis**

All graphs were generated using GraphPad Prism 6 or 8. For statistical analysis of vRootchip data, Two-way ANOVA was performed for the entire time of x-axis except for indicated ones. Welch ANOVA analysis was applied for the scanner growth assays with multiple time points, and one-way ANOVA assays were used for steady state (one time point) pH and scanner growth datasets. Stars indicate significant



differences on all graphs with ns for  $p > 0.05$ , \* for  $p \leq 0.05$ , \*\* for  $p \leq 0.01$ , \*\*\* for  $p \leq 0.001$  and \*\*\*\* for  $p \leq 0.0001$ .

## Method references

- 1 Komaki, S. *et al.* Nuclear-localized subtype of end-binding 1 protein regulates spindle organization in Arabidopsis. *J. Cell Sci* **123**, 451-459 (2010).
- 2 Marc, J. *et al.* A GFP-MAP4 reporter gene for visualizing cortical microtubule rearrangements in living epidermal cells. *Plant Cell* **10**, 1927-1939 (1998).
- 3 Robert, S. *et al.* Endosidin1 defines a compartment involved in endocytosis of the brassinosteroid receptor BRI1 and the auxin transporters PIN2 and AUX1. *PNAS* **105**, 8464-8469 (2008).
- 4 Moreno-Risueno, M.A. *et al.* Oscillating gene expression determines competence for periodic Arabidopsis root branching. *Science* **329**, 1306-11 (2010).
- 5 Martinière, A. *et al.* Uncovering pH at both sides of the root plasma membrane interface using non-invasive imaging. *PNAS*, **115**, 6488-6493 (2018).
- 6 Dharmasiri, N. *et al.* Plant development is regulated by a family of auxin receptor F box proteins. *Dev. Cell* **9**, 109-119 (2005).
- 7 Uchida, N. *et al.* Chemical hijacking of auxin signaling with an engineered auxin-TIR1 pair. *Nat. Chem. Biol.* **14**, 299 (2018).
- 8 Bennett, M. J. *et al.* Arabidopsis AUX1 gene: a permease-like regulator of root gravitropism. *Science* **273**, 948-950 (1996).
- 9 Swarup, R. *et al.* Structure-function analysis of the presumptive Arabidopsis auxin permease AUX1. *Plant Cell* **16**, 3069-3083 (2004).
- 10 Wang, R. *et al.* HSP90 regulates temperature-dependent seedling growth in Arabidopsis by stabilizing the auxin co-receptor F-box protein TIR1. *Nat. Commun.* **7**, 1-11 (2016).
- 11 Rast-Somssich, M. I. *et al.* The Arabidopsis JAGGED LATERAL ORGANS (JLO) gene sensitizes plants to auxin. *J. Exp. Bot.* **68**, 2741-2755 (2017).
- 12 Haruta, M. *et al.* Molecular characterization of mutant Arabidopsis plants with reduced plasma membrane proton pump activity. *J. Biol. Chem.* **285**, 17918-17929 (2010).
- 13 Yamauchi, S. *et al.* The plasma membrane H<sup>+</sup>-ATPase AHA1 plays a major role in stomatal opening in response to blue light. *Plant Phys.* **171**, 2731-2743 (2016).

739 14 Carbonell, A. *et al.* New generation of artificial microRNA and synthetic trans-acting small interfering RNA vectors for  
740 efficient gene silencing in Arabidopsis. *Plant Phys.* **165**, 15-29 (2014).

741 15 Karimi, M., Bleys, A., Vanderhaeghen, R. & Hilson, P. Building blocks for plant gene assembly. *Plant Phys.* **145**, 1183-  
742 1191 (2007).

743 16 Marquès-Bueno, M. M. *et al.* A versatile multisite gateway-compatible promoter and transgenic line collection for cell  
744 type-specific functional genomics in Arabidopsis. *Plant J.* **85**, 320-333 (2016).

745 17 Fuglsang, A. T. *et al.* Receptor kinase-mediated control of primary active proton pumping at the plasma membrane. *Plant*  
746 *J.* **80**, 951-964 (2014).

747 18 Dai, N., Wang, W., Patterson, S. E. & Bleecker, A. B. The TMK subfamily of receptor-like kinases in Arabidopsis display  
748 an essential role in growth and a reduced sensitivity to auxin. *PLoS One* **8**, e60990 (2013).

749 19 Wang, Q. *et al.* A phosphorylation-based switch controls TAA1-mediated auxin biosynthesis in plants. *Nat. Commun.* **11**,  
750 1-10 (2020).

751 20 Cao, M. *et al.* TMK1-mediated auxin signalling regulates differential growth of the apical hook. *Nature* **568**, 240 (2019).

752 21 Lee, J. *et al.* Type III secretion and effectors shape the survival and growth pattern of *Pseudomonas syringae* on leaf  
753 surfaces. *Plant Phys.* **158**, 1803-1818 (2012).

754 22 Fendrych, M. *et al.* Rapid and reversible root growth inhibition by TIR1 auxin signalling. *Nat. Plants* **4**, 453 (2018).

755 23 Li, L., Krens, S. G., Fendrych, M. & Friml, J. Real-time analysis of auxin response, cell wall pH and elongation in  
756 Arabidopsis thaliana hypocotyls. *Bio Protoc.* **8** (2018).

757 24 Von Wangenheim, D. *et al.* Live tracking of moving samples in confocal microscopy for vertically grown roots. *Elife* **6**,  
758 e26792 (2017).

759 25 Barbez, E., Dünser, K., Gaidora, A., Lendl, T. & Busch, W. Auxin steers root cell expansion via apoplastic pH regulation  
760 in Arabidopsis thaliana. *PNAS* **114**, E4884-E4893 (2017).

761 26 Boudaoud, A. *et al.* FibrilTool, an ImageJ plug-in to quantify fibrillar structures in raw microscopy images. *Nat. Protoc.*  
762 **9**, 457-463 (2014).

763 27 Adamowski, M., Li, L. & Friml, J. Reorientation of cortical microtubule arrays in the hypocotyl of Arabidopsis thaliana  
764 is induced by the cell growth process and independent of auxin signaling. *Int. J. Mol. Sci.* **20**, 3337 (2019).

765 28 Narasimhan, M. *et al.* Systematic analysis of specific and nonspecific auxin effects on endocytosis and trafficking. *Plant*  
766 *Phys.* **accepted**

767 29 Shabala, S. N., Newman, I. A. & Morris, J. Oscillations in H<sup>+</sup> and Ca<sup>2+</sup> ion fluxes around the elongation region of corn  
768 roots and effects of external pH. *Plant Phys.* **113**, 111-118 (1997).

769 30 De Rybel, B. *et al.* A bHLH complex controls embryonic vascular tissue establishment and indeterminate growth in  
770 Arabidopsis. *Dev. Cell* **24**, 426-437 (2013).

771 31 Wendrich, J. R., Boeren, S., Möller, B. K., Weijers, D. & De Rybel, B. in *Plant Hormones*: 147-158 (Springer, 2017).

772 32 Nikonorova, N. *et al.* Early mannitol-triggered changes in the Arabidopsis leaf (phospho)proteome reveal growth  
773 regulators. *J. Exp. Bot.* **69**, 4591-4607 (2018).

774 33 Hayashi, Y. *et al.* Biochemical characterization of in vitro phosphorylation and dephosphorylation of the plasma  
775 membrane H<sup>+</sup>-ATPase. *Plant Cell Physiol.* **51**, 1186-1196 (2010).

776 34 Inoue, S.-i., Takahashi, K., Okumura-Noda, H. & Kinoshita, T. Auxin influx carrier AUX1 confers acid resistance for  
777 Arabidopsis root elongation through the regulation of plasma membrane H<sup>+</sup>-ATPase. *Plant Cell Physiol.* **57**, 2194-2201  
778 (2016).

779 35 Spartz, A. K. *et al.* SAUR inhibition of PP2C-D phosphatases activates plasma membrane H<sup>+</sup>-ATPases to promote cell  
780 expansion in Arabidopsis. *Plant Cell* **26**, 2129-2142 (2014).

781 36 Walter, M. *et al.* Visualization of protein interactions in living plant cells using bimolecular fluorescence  
782 complementation. *Plant J.* **40**, 428-438 (2004).

783 37 Leuzinger, K. *et al.* Efficient agroinfiltration of plants for high-level transient expression of recombinant proteins. *J. Vis.*  
784 *Exp.* **77**: 50521 (2013).

785 38 Czechowski, T., Stitt, M., Altmann, T., Udvardi, M. K. & Scheible, W.-R. Genome-wide identification and testing of  
786 superior reference genes for transcript normalization in Arabidopsis. *Plant Phys.* **139**, 5-17 (2005).

## Acknowledgements

We thank Nadine Paris for sharing the PM-Cyto seeds, Lukas Hörmayer for help with the auxin sensitivity assay analysis. This research was possible thanks to the Scientific Service Units (SSU) of IST-Austria through resources provided by the Bioimaging Facility (BIF). In particular, we are grateful to Judit Singer for improving the vertical microscope stage for the vRootchip imaging chamber, to Yann Cesbron for modifying the ratiometric fluorescence script for pH analysis and to Robert Hauschild for modifying the Fibril tool script for CMT analysis. The Austria IST machine shop we thank for constructing the vRootchip imaging chamber. This project has received funding from the European Research Council Advanced Grant (ETAP-742985), the Austrian Science Fund (FWF) I 3630-B25, and the National Institutes of Health (GM067203 to W.M.G.). W.S. and B.D.R. were funded by the Netherlands Organization for Scientific Research (NWO; VIDI-864.13.001), The Research Foundation - Flanders (FWO; Odysseus II G0D0515N) and a European Research Council Starting Grant (TORPEDO-714055). M.R. and D.W. were funded by a VICI grant (865.14.001) from the Netherlands Organization for Scientific Research. S.S. acknowledges the financial support from the Australian Research Council and China National Distinguished Expert Project (WQ20174400441). K.T. (20K06685) and T.K. (20H05687 and 20H05910) were funded by MEXT/JSPS KAKENHI. L.L. was funded by the European Union's Horizon 2020 research and innovation programme under the Marie Skłodowska-Curie Grant Agreement No. 665385 and the DOC Fellowship of the Austrian Academy of Sciences.

## Author contributions.

L.L., I.V. and J.F. conceived and designed the experiments. L.L. and I.V. carried out most of the experiments and analysis. M.R. and D.W. performed the phospho-proteomics analysis and TIR1 and AFB1 IP-MS/MS. I.V., W.S. and B.D.R. performed TMK1 IP-MS/MS experiments and statistical analysis. MS/MS analysis was performed by the VIB Proteomics Core. L.S. and S.S. performed MIFE experiments. K.T. and T.K. did the ATP hydrolysis assays. J.C. and S.V. created and shared the *AtTAS1c-AHA* lines.

L.R. and L.L. created transgenic lines and crosses. H.R. and W.M.G. conducted leaf wilting phenotype analysis, western blot of *tmk1,4*, shared plasmids, seeds materials and contributed to discussion of the results. J.M. and L.L. modified the microfluidic chip. L.L, I.V. and J.F. wrote the manuscript.

### **Competing interests.**

The authors declare no competing interests.

### **Additional information and correspondence**

The main data supporting the findings of this study are available within the paper and its Extended Information. Additional data are available from the corresponding authors upon reasonable request. Correspondence and requests for materials should be addressed to J.F.

## Extended Data Figure/Table Legends

### Extended Data Figure 1. Investigation of cellular mechanisms potentially involved in auxin-induced rapid root growth inhibition.

**a-b**, Dynamic cortical microtubule (CMT) reorientation in root cells from transversal to longitudinal in response to 100 nM IAA treatment. CMT was imaged in late elongating epidermal cells in the *pEB1b::EB1-GFP* marker line in vRootchip. Scans were made at 6.25 second intervals and a max Z-projection of 10 subsequent time frames was analysed using the FibrilTool macro. The average orientation of the microtubules is represented by the slope of the red line and the length of the line represents its anisotropy **(a)**. Quantification of CMT reorientation after 100 nM IAA treatment in **(a)**. The percentage of CMT reorientation at every time point is calculated as the difference in the angle of that time point and the initial time point divided by the difference in the angles of the initial time point and end time point at 42 minutes. Mean of 5 elongating cells,  $\pm$  SD **(b)**.

**c-e**, Analysis of CMT reorientation in elongating epidermal root cells **(c, d)** and root growth **(e)** of *35S::MAP4-GFP* in response to 10 nM IAA, 10  $\mu$ M taxol and IAA+taxol co-treatment. Orientation of CMT was analysed with the Bioline script. Green-colored CMTs mark transversal oriented CMT (angle between  $-45^\circ$  and  $+45^\circ$ ), while red-colored CMTs indicate longitudinal orientation (angle between  $+45^\circ$  and  $135^\circ$ ). Scale bar = 15  $\mu$ m **(c)**. Quantification of **(c)** as the percentage of longitudinal CMT to total CMT detected.  $n > 11$ , One-way ANOVA **(d)**. Growth on respective treatments for 2 hours were measured.  $n > 10$ , One-way ANOVA **(e)**. \* $p \leq 0.05$ , \*\*\*\* $p \leq 0.0001$ .

**f**, Vacuolar morphology tracked in the *pSYP22::SYP22-YFP* marker line (green signal) in the same elongating cells before and after 30 minutes of 100 nM IAA. Scale bar = 15  $\mu$ m. Magenta signal indicates propidium-iodide stained cell walls.

**g**, Dynamics of apoplastic pH measured in different cells across the whole EZ (p1-p8) in vRootchip. The TL and blue-yellow scale image are from the same sample shown in **Fig. 1a**. Scale bar= 30  $\mu$ m. The upper charts depict the dynamics of apoplastic pH in the indicated cells in response to 5 nM IAA, and the lower

charts represent the pH in response to washout. The left two charts show the apoplastic pH measured by the HPTS dye. The right two charts show the speed at which each cell reaches its maximum pH change calculated as the difference between the pH at a given time point and the pre-stimulus pH, divided by the end pH change in that cell.

**h**, Dynamics of root surface pH and medium pH in vRootchip. Left graph shows the elongation zone of the root. The ROIs p1-p5 were chosen along the root, 30  $\mu$ m away from the root surface indicated by the vertical white dotted line, while ROIs p6-p9 were distanced away from the root. The pH at the surface of the root (vertical positions p1-p5) increased after IAA and recovered after washout within 30 seconds. In contrast, the pH away from the root surface did not change significantly (horizontal positions p6-p9).

**i**, PM H<sup>+</sup>-net influx measured by a non-invasive microelectrode before and after 10 nM IAA treatment in the elongating zone of WT roots. Means of 9 roots  $\pm$  SD.

**j-k**, The medium pH (**j**) and apoplastic pH (**k**) changed rapidly after the exchange of the medium of different pH in vRootchip. Following media were used sequentially: basal medium at pH 5.8, auxin-containing medium at pH 5.8, gradually more acidic medium of pH 5.6, followed by pH 5.4 and lastly again basal medium at pH 5.8.

**l**, Quantification of root growth rate in response to the gradual addition of KOH in the medium in the vRootchip. The greener the shade, the more KOH was added followed by washout with the initial basal pH 5.8 medium.

**m**, Scheme of the modified vRootchip adding valve 6 and with valve routes adjusted.

## **Extended Data Figure 2. H<sup>+</sup>-ATPase activation counteracts auxin-mediated apoplast alkalinisation and growth inhibition**

**a**, Measurement of luminescence intensity on the root tip of *DR5::LUC* line after 10  $\mu$ M FC, 10 nM IAA and IAA+FC co-treatment.  $n > 3$ . IAA and IAA+FC are significantly different from the mock ( $p \leq 0.0001$ ). No significant difference between IAA and IAA+FC ( $p > 0.05$ ). Two-way ANOVA.

**b-g**, FC and IAA counteract each other. Addition of IAA still increased apoplastic pH (**b**) and inhibited root growth (**c**) in presence of FC in vRootchip.  $n = 4$  (**b**, **c**). Addition of FC still decreased the apoplastic pH (**d**) and promoted root growth (**e**) in presence of IAA in vRootchip.  $n = 4$ , the shaded area represents the duration time of the indicated treatments (**d-e**). Root growth after FC, IAA and co-treatment for 1 hour in steady state by scanner. 1  $\mu$ M FC and 10 nM IAA were used in (**f**) while 10  $\mu$ M FC and 2 nM IAA were used in (**g**).  $n > 9$  for both graphs, ns  $p > 0.05$ , \* $p \leq 0.05$ , \*\* $p \leq 0.01$ , \*\*\*\* $p \leq 0.0001$ , One-way ANOVA (**f-g**). **h**, Dose-response of auxin-induced root growth inhibition of *aha* single mutants.  $n > 22$ . Relative GR is ratio between auxin-affected growth in the mutant to mock growth for the same genotype. ns  $p > 0.05$ , \*\* $p \leq 0.01$ , \*\*\* $p \leq 0.001$ , Welch ANOVA. **i**, Quantitative Real-time PCR on the *AHA1,2,7,11* expression in root tips of *AtTAS1c-AHA#2* and *#4*. The expression level was normalized to *EFL1* as housekeeping gene. Means of 3 biological replicates + SD.

### **Extended Data Figure 3. TMK1 directly mediates auxin-induced H<sup>+</sup>-ATPase activation.**

**a**, IP-MS/MS on *pTIR1::TIR1-VENUS* in *tir1-1* and *pAFB1::AFB1-VENUS* in *afb1-3* lines under normal condition (upper graphs) compared to 1 hour 50  $\mu$ M MG132 pre-incubation and 100nM IAA treatment for 2 minutes (lower graphs). Volcano plots show fold changes (in  $\log^2$  scale, x-axis) and significance (p-value, y-axis). Proteins passing the threshold of FDR 0.05 and specific fold change are marked. Green depicts the respective bait protein and red depicts known members of the SCF E3 ubiquitin ligase complex. Pulldowns were performed in triplicate, LFQ analysis.

**b**, IP-MS/MS on *35S::TMK1-GFP* line. Volcano plot shows fold change (in  $\log^{10}$  scale, x-axis) and significance (p-value, y-axis). Red dots are in the range of ratio  $> 10$  and  $-\text{LOG } p\text{-value} > 2$ . P-values are calculated based on the three replicates of *35S::TMK1-GFP* vs WT using a Two-sided t-test.

**c**, co-IP of *pTMK1::TMK1-GFP* roots, followed by Western blot detection of AHA2 and Thr<sup>947</sup>-phosphorylated AHA2. The interaction was not regulated by 30 minutes of 100 nM IAA treatment, but the phosphorylation state of the interacting AHA2 was increased.



**d**, Bimolecular Fluorescent Complementation (BiFC) in *Nicotiana benthamiana* leaves transiently transformed with *YFP<sup>N</sup>-TMK1*, *AHA2-YFP<sup>C</sup>* or both. Scale bar = 10µm

**e**, Representation of wilting leaves of *Nicotiana benthamiana* that transiently express the WT TMK1 and ATP-site mutated forms: *p35S::TMK1-HA K<sup>616</sup>E* or *K<sup>616</sup>R*.

**f**, Western blot analysis of the AHA2 levels and the Thr<sup>947</sup> phosphorylation in roots of *DEX::TMK1<sup>K616R</sup>-HA* and *DEX::TMK1-HA* lines treated +/- DEX (30 µM for 24 hours) and +/- IAA (100 nM for 1 hour).

**g-h**, Western blot detection of the AHA2 levels and the Thr<sup>947</sup> phosphorylation in *tmk1,3* roots treated with 100 nM IAA for 1 hour (**g**). Quantification of the auxin effect on AHA2 phosphorylation in (**g**) by normalising the intensity ratio of pThr<sup>947</sup> to AHA2 detected in auxin-treated roots to the same ratio in mock-treated samples of the same genotype (**h**).

**Extended Data Figure 4. TIR1/AFB and TMK1 signalling converge antagonistically on apoplastic pH and growth regulation.**

**a-b**, Apoplastic alkalinisation (**a**) and root growth inhibition (**b**) in response to IAA measured in *aux1-100* mutant compared to WT roots in vRootchip. Apoplastic pH is measured by the HPTS dye. *n* = 3; *p* ≤ 0.0001, Two-way ANOVA for both graphs.

**c-d**, Apoplastic alkalinisation (**c**) and root growth inhibition (**d**) in response to the synthetic auxin analogue 2,4-D in *aux1-100* mutant compared to WT roots. The steady state pH with the HPTS dye was measured 30 minutes after mock or 100 nM 2,4-D treatment. *n* > 6, One-way ANOVA (**c**). The growth obtained in 2 hours was captured by scanner. *n* > 4, One-way ANOVA (**d**). ns *p* > 0.05, \*\**p* ≤ 0.01, \*\*\**p* ≤ 0.001.

**e**, Root growth of *tir triple* mutant (in red) compared to WT (in black) in response to 5 nM IAA in the vRootchip. *n* = 3, 2. *p* ≤ 0.0001, two-way ANOVA.

**f-g**, apoplastic pH (**f**) and root growth (**g**) after 10 µM PEO-IAA and 5 nM IAA. The steady state pH was measured 30 minutes after the treatments using the HPTS dye, while the root growth obtained in 1 hour was recorded by scanning the plates. *n* > 7, ns *p* > 0.05, \*\**p* ≤ 0.01, \*\*\*\**p* ≤ 0.0001, One-way ANOVA.

**h**, Dose-response of auxin-induced root growth inhibition of *pUBQ10::TMK1-3HA* compared to WT and *tmk1-1*. Relative GR is the ratio between auxin-affected growth in a mutant to the mock growth for the same genotype.  $n > 7$ . ns  $p > 0.05$ , \* $p \leq 0.05$ , Welch ANOVA.

**i-j**, Raw data for **Figure 4d** and **e**, respectively. ns  $p > 0.05$ , \*\* $p \leq 0.01$ , \*\*\*\* $p \leq 0.0001$ , One-way ANOVA.

**Extended Data Table 1. Phospho-proteomic data of rapid auxin effects in root and phospho-proteomic analysis of H<sup>+</sup>-ATPases in *tmk1-1* mutants**

Table contains differentially regulated phospho-peptides (FDR  $\leq 0.05$ ) in H<sup>+</sup>-ATPases in IAA treated versus mock-treated roots. IAA treatment was at 100 nM for 2 minutes. QHF and LTQXL analysis are given in Tab 1 and 2, respectively. Tab 3 shows the differentially phosphorylated phospho-sites of AHAs in *tmk1-1* background compared to WT.

**Extended Data Table 2. IP-MS analysis of pTIR1::TIR1-VENUS and pAFB1::AFB1-VENUS**

Overview of the putative TIR1 and AFB1 interactors after MaxQuant and Perseus statistical analysis. Samples were TIR1 and AFB1-Venus lines under mock, 50  $\mu$ M MG132 pre-incubation for 1 hour and 100 nM IAA treatment for 2 minutes. Proteins passing the threshold of FDR 0.05 and specific fold change are included in the table. P-values are calculated based on the three replicates using a Two-sided t-test. Pulldowns were performed in triplicate. Yellow highlight indicates the respective bait protein.

**Extended Data Table 3. IP-MS analysis of p35S::TMK1-GFP.**

Overview of the putative TMK1 interactors after MaxQuant and Perseus statistical analysis. The list is sorted based on the ratio of 35S::TMK1-GFP vs WT control. Proteins passing the threshold of FDR 0.05 and specific fold change are included in the table. P-values are calculated based on the three replicates using a two-sided t-test. Yellow highlight indicates bait, green indicates GFP and orange indicates selected proteins.



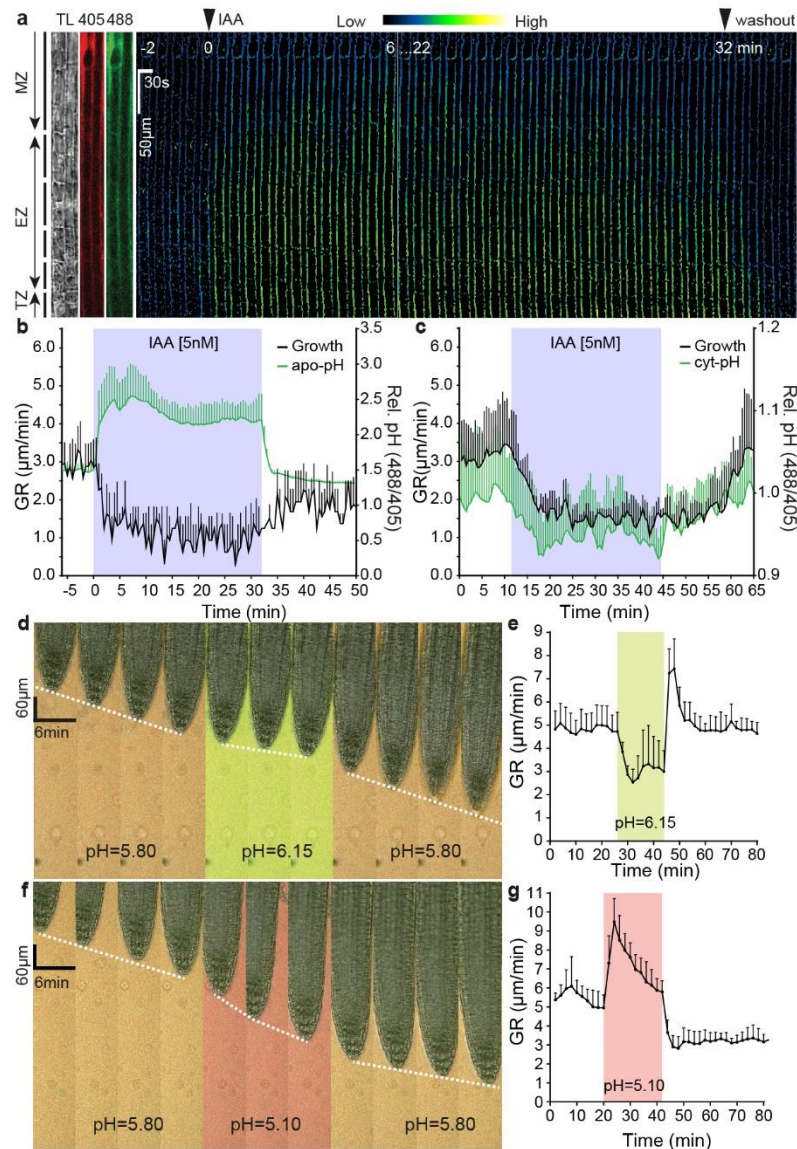


**Figure 1. Auxin rapidly inhibits root growth by alkalinising the apoplast**

**a**, Time lapse of the apoplastic pH response in root tip epidermal cells to 5 nM IAA treatment followed by auxin washout (basal auxin-free medium) in vRootchip. pH was monitored in the same region of interest (ROI) for 36 minutes by the ratiometric HPTS dye. The ratio-image represents the ratio of excitation 488 nm and 405 nm. ROI covers maturation zone (MZ), elongation zone (EZ) and transition zone (TZ). TL is transmitted light image.

**b**, Quantitative analysis of the auxin-induced apoplast alkalinisation in the EZ reported by HPTS dye and corresponding inhibition and recovery of root tip growth rate (GR) following 5 nM IAA and washout as in (a). Means of 4 roots + SD.

**c**, Quantitative analysis of the auxin-induced cytoplasm acidification in the EZ, visualized by the PM-cyto reporter and the corresponding inhibition and recovery of GR upon 5 nM IAA treatment and washout in vRootchip. Means of 3 roots +SD.

**d-g**, Time-lapse of root growth response to a pulse of alkaline (pH 6.15) (d) or acidic medium (pH 5.10) (f). The slope of the white dotted line that tracks the root tip indicates the GR. Quantifications of GR in d (n = 8) (e) and f (n = 7) (g). The shaded areas represent the duration of the indicated treatments. Mean +SD.

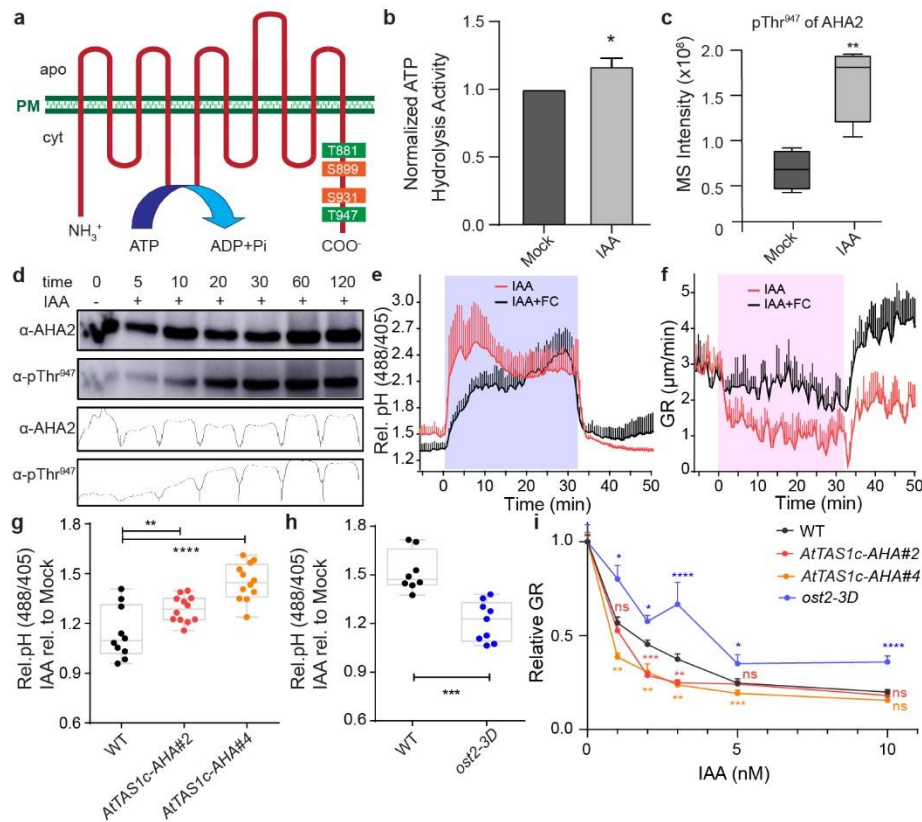


**Figure 2. Auxin-triggered H<sup>+</sup>-ATPase phosphorylation and activation counteract auxin-mediated apoplast alkalisation and growth inhibition**

**a**, Representation of the phospho-sites in the model of the *Arabidopsis thaliana* H<sup>+</sup>-ATPase 2 (AHA2) identified in the phospho-proteomic analysis of auxin-treated root samples (2 minutes of 100 nM IAA). The color reflects their impact on the H<sup>+</sup>-translocation activity (green for activation and orange for inhibition).

**b**, Quantification of ATP hydrolysis induction in root samples treated with 100 nM IAA for 1 hour in comparison to mock-treated roots. The IAA-treated sample was normalized by the corresponding mock-treated sample. Bars indicate means of 3 biological replicates + SD. Unpaired t-test. \*  $p \leq 0.05$ .

**c**, Phospho-proteome detection of auxin-induced AHA2-Thr<sup>947</sup> phosphorylation after 2 minutes of 100 nM IAA treatment.  $n = 4$ . Box plot depicts minimum to maximum, mean  $\pm$  SD. Two-sample t-test (part of MaxQuant-Perseus analysis). \*\*  $p \leq 0.01$ .

**d**, Time-course western blot analysis of auxin-induced Thr<sup>947</sup>-phosphorylated AHA2 levels in roots treated with 10 nM IAA using AHA2 and pThr<sup>947</sup>-specific antibodies. Total AHA2 protein levels were monitored in the same samples as a control. Band intensities of the different lanes are quantified by the Gels Analysis function in ImageJ.

**e-f**, Apoplastic pH (**e**) and root growth (**f**) analysis upon pharmacological activation of H<sup>+</sup>-pumps by 10  $\mu$ M FC and 10 nM IAA in vRootchip. Apoplastic pH was monitored using HPTS. The shaded area represents the duration of the indicated treatment. Mean of 4 roots for each treatment + SD.  $p \leq 0.0001$  between IAA and IAA+FC, from 0 – 32 min (**e**), from 0 – 31 min (**f**), Two-way ANOVA.

**g-h**, Apoplastic pH response in two independent AHA knock-down lines (*AtTAS1c-AHA#2* and #4) ( $n > 9$ ) (**g**), and the *ost2-3D* gain-of-function allele ( $n > 5$ ) (**h**) in response to 30 minutes 5 nM IAA treatment. Apoplastic pH changes are determined by the HPTS dye and IAA treatment was normalized to the corresponding mock-treatment. \*\*  $p \leq 0.01$ , \*\*\*  $p \leq 0.001$ , \*\*\*\*  $p \leq 0.0001$ , One-way ANOVA.

**i**, Dose-response of auxin-induced root growth inhibition of *AtTAS1c-AHA* lines and *ost2-3D* mutants reveals hypersensitivity and resistance respectively to IAA in comparison to WT ( $n > 15$ ) (**i**). The relative

994 GR is calculated by the ratio of GR for each IAA concentration relative to mock-treated GR of the same  
995 genotype. \* $p \leq 0.05$ , \*\* $p \leq 0.01$ , \*\*\* $p \leq 0.001$ , \*\*\*\* $p \leq 0.0001$ , Welch ANOVA.

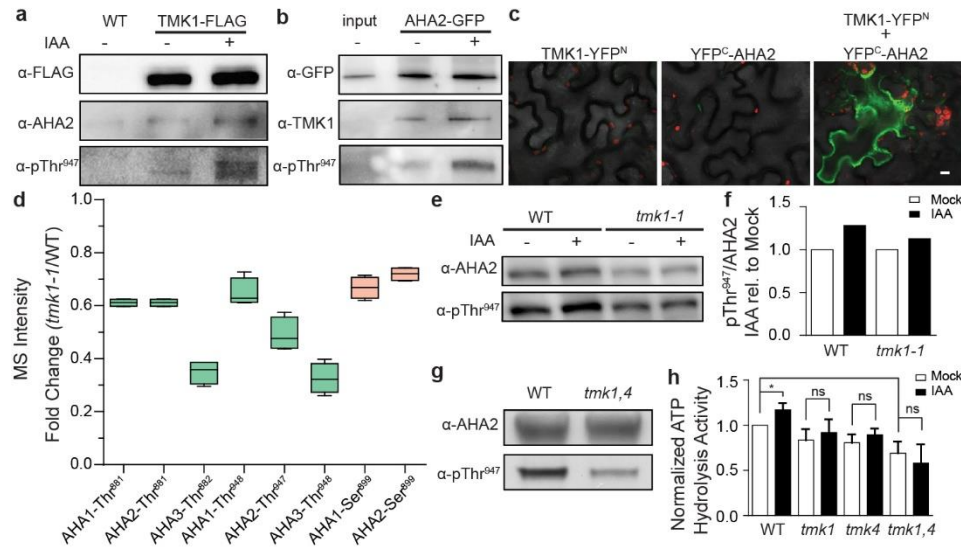


**Figure 3. TMK1 directly mediates auxin-induced H<sup>+</sup>-ATPase activation.**

**a**, Co-immunoprecipitation (co-IP) of the *pTMK1::TMK1-FLAG* from roots mock or 100 nM IAA-treated for 30 minutes, followed by Western blot detection of AHA2 and Thr<sup>947</sup>-phosphorylated AHA2. The control is the co-IP of WT (Col-0) roots.

**b**, Co-IP of *pAHA2::AHA2-GFP* from roots, followed by Western blot detection of TMK1 and Thr<sup>947</sup>-phosphorylated AHA2 on roots mock or 100 nM IAA-treated for 30 minutes. Interaction does not depend on auxin presence, but auxin-induced phosphorylation of the interacting AHA2 was observed. As a control sample we include input of *pAHA2::AHA2-GFP* roots.

**c**, Bimolecular Fluorescent Complementation (BiFC) in *Nicotiana benthamiana* leaves transiently transformed either with *TMK1-YFP<sup>N</sup>* (*TMK1* in *pSPYNE*), *YFP<sup>C</sup>-AHA2* (*AHA2* in *pSPYCE*) or both. Scale bar = 10  $\mu$ m.

**d**, Differentially detected phospho-sites of AHAs in *tmk1-1* normalized to WT (Col-0) MS detection levels. We observe less phosphorylation on the indicated phospho-sites in AHA1, AHA2 and AHA3 in the *tmk1-1* mutant. Green indicates the sites with known activation function, while orange is used for known inhibitory function. n= 4. Box plot depicts minimum to maximum, mean  $\pm$  SD. Two-sample t-test (part of MaxQuant-Perseus analysis).

**e**, Western blot analysis of auxin-induced AHA2 Thr<sup>947</sup> phosphorylation in WT and *tmk1-1* roots treated with 100 nM IAA for 1 hour. AHA2 levels were determined as a control.

**f**, Quantification of the auxin effect on AHA2 phosphorylation in (d) by normalising the intensity ratio of pThr<sup>947</sup> to AHA2 in auxin-treated root samples to the same ratio in mock-treated samples of the respective genotypes.

**g**, Western blot detection of the AHA2 levels and its Thr<sup>947</sup> phosphorylation in full seedlings shows reduced AHA2 phosphorylation in *tmk1,4* compared to WT.

**h**, Auxin-induced ATP hydrolysis activity is impaired in *tmk* mutants relative to WT roots (1 hour mock or 100 nM IAA treatment). The IAA-treated sample was normalized to the mock-treated WT. Means of 3 biological replicates + SD. \* $p \leq 0.05$ , ns  $p > 0.05$ , One-way ANOVA.



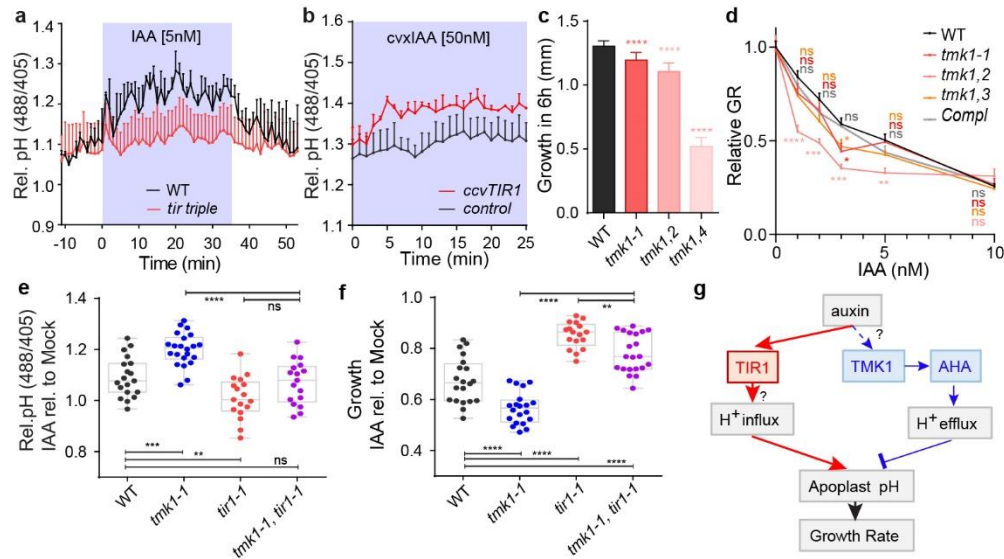


**Figure 4. TIR1/AFB and TMK1 signalling converge antagonistically on apoplastic pH and growth regulation.**

**a**, Apoplastic pH analysis by the HPTS dye shows an impaired auxin response (to 5nM IAA) in *tir triple* mutant roots (in red) compared to WT roots (in black) in vRootchip. Means of 3, 2 roots + SEM.  $p \leq 0.0001$ , Two-way ANOVA.

**b**, Apoplastic pH analysis by the HPTS dye shows apoplastic alkalinisation in *ccvTIR1* line (in red) compared to the *control* line (in black) in response to cvxIAA in vRootchip. Means of 2, 3 roots + SEM.  $p \leq 0.01$ , from 0 - 5 minutes, Two-way ANOVA. The shaded area represents the duration of the indicated treatment.

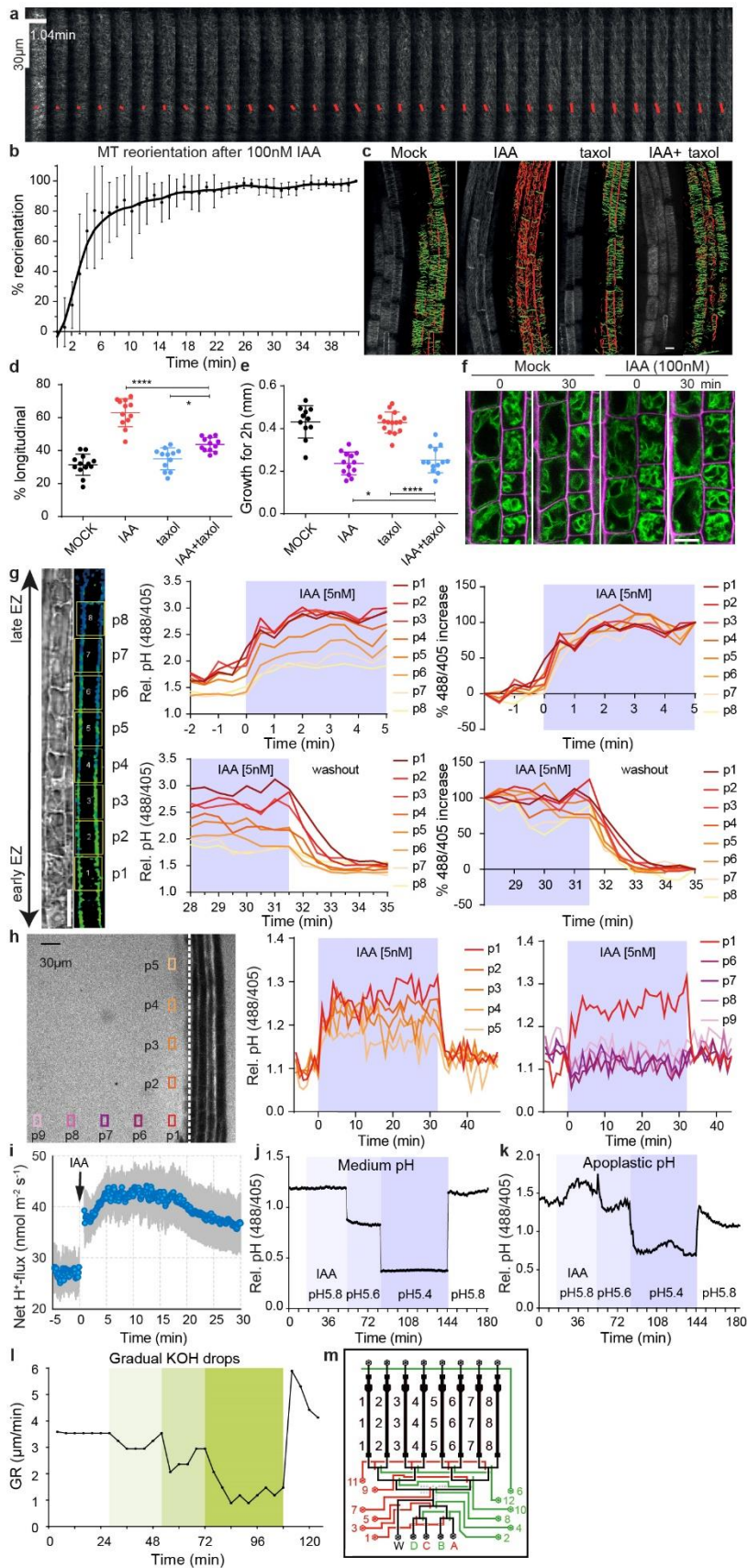
**c**, Steady-state root growth over 6 hours in *tmk1*-related mutants.  $n = 6$  for *tmk1,4*;  $n > 26$  for others. \*\*\*\* $p \leq 0.0001$ , One-way ANOVA.

**d**, Dose-response of auxin-induced root growth inhibition of *tmk1*-related mutants relative to WT and a complementary line (*pTMK1::TMK1-FLAG* in *tmk1-1*). Relative GR is the ratio between auxin-affected growth and mock growth for the same genotype.  $n > 15$ . \* $p \leq 0.05$ , \*\* $p \leq 0.01$ , \*\*\* $p \leq 0.001$ , \*\*\*\* $p \leq 0.0001$ , Welch ANOVA.

**e-f**, Apoplastic pH (**e**) and root growth (**f**) measurement in *tmk1-1*, *tir1-1* and *tmk1-1,tir1-1* mutants in response to 5 nM IAA. The apoplastic pH is indicated by the HPTS emission ratio after 50 minutes treatment. The root growth is measured after 6 hours.  $n > 16$  for both graphs, ns  $p > 0.05$ , \*\* $p \leq 0.01$ , \*\*\* $p \leq 0.001$ , \*\*\*\* $p \leq 0.0001$ , one-way ANOVA.

**g**, Model for auxin-mediated root growth regulation. Auxin induces rapid  $H^+$ -influx across the PM to alkalinise the apoplast and inhibit root growth through an intracellular, non-transcriptional branch of the TIR1/AFB signalling pathway. Concomitantly, auxin through cell surface TMK1 activates  $H^+$ -pumps (AHAs) to promote  $H^+$ -efflux to acidify apoplast and promote growth.





**Extended Data Figure 1. Investigation of cellular mechanisms potentially involved in auxin-induced rapid root growth inhibition.**

**a-b**, Dynamic cortical microtubule (CMT) reorientation in root cells from transversal to longitudinal in response to 100 nM IAA treatment. CMT was imaged in late elongating epidermal cells in the *pEB1b::EB1-GFP* marker line in vRootchip. Scans were made at 6.25 second intervals and a max Z-projection of 10 subsequent time frames was analysed using the FibrilTool macro. The average orientation of the microtubules is represented by the slope of the red line and the length of the line represents its anisotropy (**a**). Quantification of CMT reorientation after 100 nM IAA treatment in (**a**). The percentage of CMT reorientation at every time point is calculated as the difference in the angle of that time point and the initial time point divided by the difference in the angles of the initial time point and end time point at 42 minutes. Mean of 5 elongating cells,  $\pm$  SD (**b**).

**c-e**, Analysis of CMT reorientation in elongating epidermal root cells (**c**, **d**) and root growth (**e**) of *35S::MAP4-GFP* in response to 10 nM IAA, 10  $\mu$ M taxol and IAA+taxol co-treatment. Orientation of CMT was analysed with the Bioline script. Green-colored CMTs mark transversal oriented CMT (angle between  $-45^\circ$  and  $+45^\circ$ ), while red-colored CMTs indicate longitudinal orientation (angle between  $+45^\circ$  and  $135^\circ$ ). Scale bar = 15  $\mu$ m (**c**). Quantification of (**c**) as the percentage of longitudinal CMT to total CMT detected.  $n > 11$ , One-way ANOVA (**d**). Growth on respective treatments for 2 hours were measured.  $n > 10$ , One-way ANOVA (**e**). \* $p \leq 0.05$ , \*\*\*\* $p \leq 0.0001$ .

**f**, Vacuolar morphology tracked in the *pSYP22::SYP22-YFP* marker line (green signal) in the same elongating cells before and after 30 minutes of 100 nM IAA. Scale bar = 15  $\mu$ m. Magenta signal indicates propidium-iodide stained cell walls.

**g**, Dynamics of apoplastic pH measured in different cells across the whole EZ (p1-p8) in vRootchip. The TL and blue-yellow scale image are from the same sample shown in **Fig. 1a**. Scale bar = 30  $\mu$ m. The upper charts depict the dynamics of apoplastic pH in the indicated cells in response to 5 nM IAA, and the lower charts represent the pH in response to washout. The left two charts show the apoplastic pH measured by the HPTS dye. The right two charts show the speed at which each cell reaches its maximum pH change calculated as the difference between the pH at a given time point and the pre-stimulus pH, divided by the end pH change in that cell.

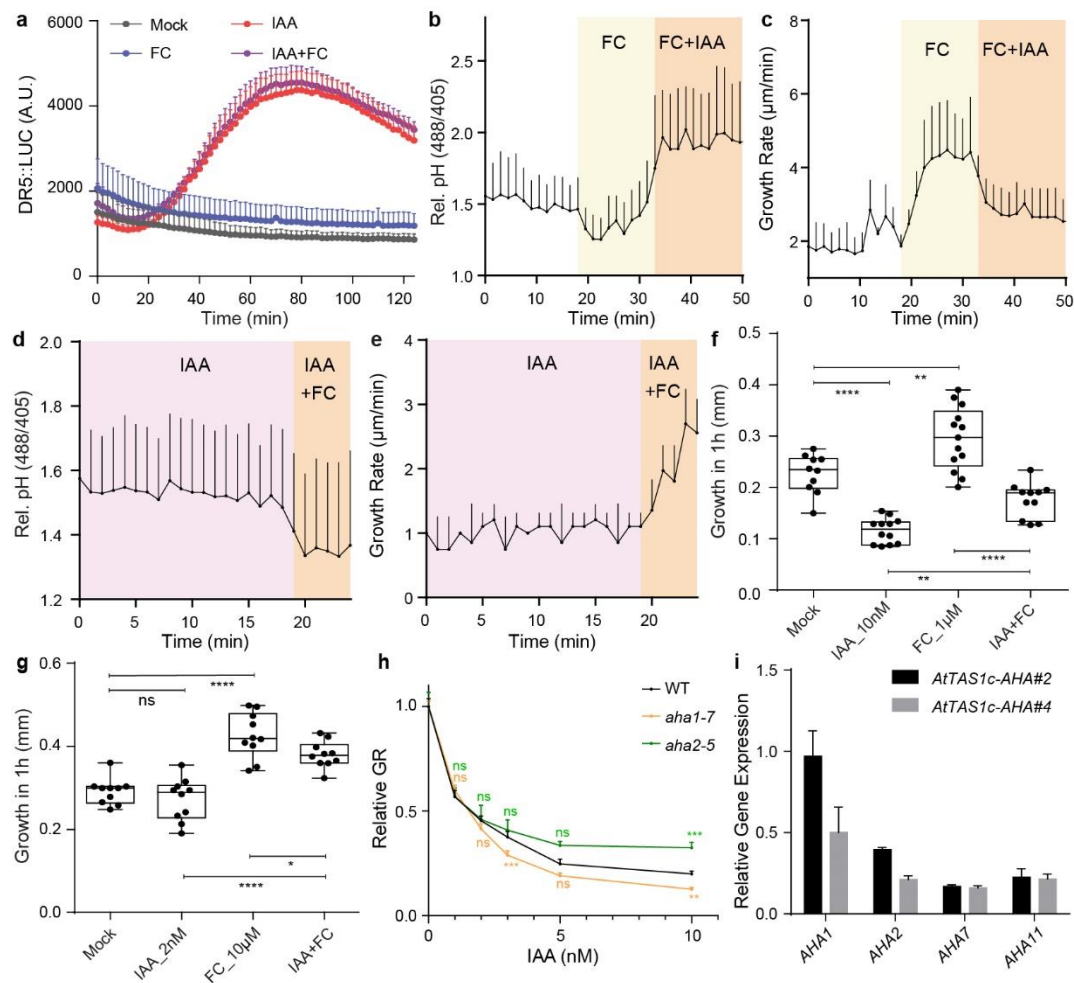
**h**, Dynamics of root surface pH and medium pH in vRootchip. Left graph shows the elongation zone of the root. The ROIs p1-p5 were chosen along the root, 30  $\mu$ m away from the root surface indicated by the vertical white dotted line, while ROIs p6-p9 were distanced away from the root. The pH at the surface of the root (vertical positions p1-p5) increased after IAA and recovered after washout within 30 seconds. In contrast, the pH away from the root surface did not change significantly (horizontal positions p6-p9).

**i**, PM  $H^+$ -net influx measured by a non-invasive microelectrode before and after 10 nM IAA treatment in the elongating zone of WT roots. Means of 9 roots  $\pm$  SD.

**j-k**, The medium pH (**j**) and apoplastic pH (**k**) changed rapidly after the exchange of the medium of different pH in vRootchip. Following media were used sequentially: basal medium at pH 5.8, auxin-containing medium at pH 5.8, gradually more acidic medium of pH 5.6, followed by pH 5.4 and lastly again basal medium at pH 5.8.

**l**, Quantification of root growth rate in response to the gradual addition of KOH in the medium in the vRootchip. The greener the shade, the more KOH was added followed by washout with the initial basal pH 5.8 medium.

**m**, Scheme of the modified vRootchip adding valve 6 and with valve routes adjusted.



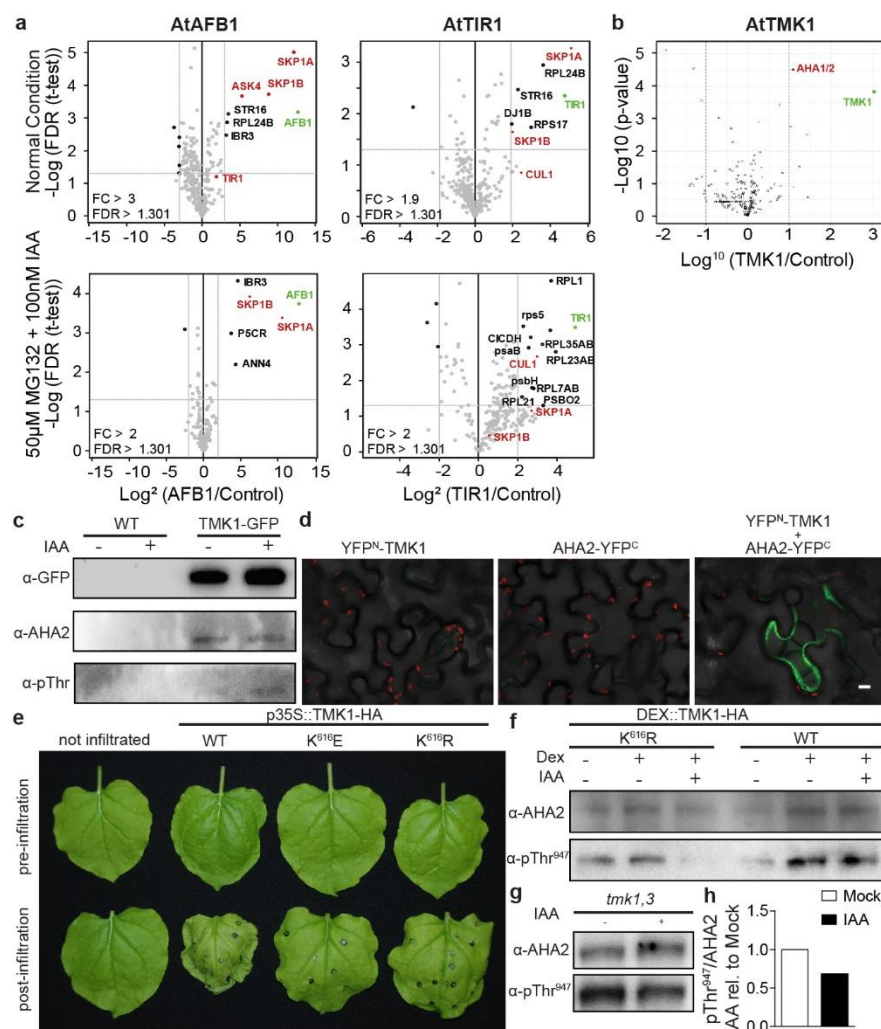
## Extended Data Figure 2. H<sup>+</sup>-ATPase activation counteracts auxin-mediated apoplast alkalinisation and growth inhibition

**a**, Measurement of luminescence intensity on the root tip of *DR5::LUC* line after 10  $\mu\text{M}$  FC, 10 nM IAA and IAA+FC co-treatment.  $n > 3$ . IAA and IAA+FC are significantly different from the mock ( $p \leq 0.0001$ ). No significant difference between IAA and IAA+FC ( $p > 0.05$ ). Two-way ANOVA.

**b-g**, FC and IAA counteract each other. Addition of IAA still increased apoplastic pH (**b**) and inhibited root growth (**c**) in presence of FC in vRootchip.  $n = 4$  (**b**, **c**). Addition of FC still decreased the apoplastic pH (**d**) and promoted root growth (**e**) in presence of IAA in vRootchip.  $n = 4$ , the shaded area represents the duration time of the indicated treatments (**d-e**). Root growth after FC, IAA and co-treatment for 1 hour in steady state by scanner. 1  $\mu\text{M}$  FC and 10 nM IAA were used in (**f**) while 10  $\mu\text{M}$  FC and 2 nM IAA were used in (**g**).  $n > 9$  for both graphs, ns  $p > 0.05$ , \* $p \leq 0.05$ , \*\* $p \leq 0.01$ , \*\*\*\* $p \leq 0.0001$ , One-way ANOVA (**f-g**).

**h**, Dose-response of auxin-induced root growth inhibition of *aha* single mutants.  $n > 22$ . Relative GR is ratio between auxin-affected growth in the mutant to mock growth for the same genotype. ns  $p > 0.05$ , \*\* $p \leq 0.01$ , \*\*\* $p \leq 0.001$ , Welch ANOVA.

**i**, Quantitative Real-time PCR on the *AHA1,2,7,11* expression in root tips of *AtTAS1c-AHA#2* and #4. The expression level was normalized to *EF1a* as housekeeping gene. Means of 3 biological replicates + SD.



### Extended Data Figure 3. TMK1 directly mediates auxin-induced H<sup>+</sup>-ATPase activation.

**a**, IP-MS/MS on *pTIR1::TIR1-VENUS* in *tir1-1* and *pAFB1::AFB1-VENUS* in *afb1-3* lines under normal condition (upper graphs) compared to 1 hour 50 μM MG132 pre-incubation and 100nM IAA treatment for 2 minutes (lower graphs). Volcano plots show fold changes (in log<sup>2</sup> scale, x-axis) and significance (p-value, y-axis). Proteins passing the threshold of FDR 0.05 and specific fold change are marked. Green depicts the respective bait protein and red depicts known members of the SCF E3 ubiquitin ligase complex. Pulldowns were performed in triplicate, LFQ analysis.

**b**, IP-MS/MS on *35S::TMK1-GFP* line. Volcano plot shows fold change (in log<sup>10</sup> scale, x-axis) and significance (p-value, y-axis). Red dots are in the range of ratio > 10 and -LOG p-value > 2. P-values are calculated based on the three replicates of *35S::TMK1-GFP* vs WT using a Two-sided t-test.

**c**, co-IP of *pTMK1::TMK1-GFP* roots, followed by Western blot detection of AHA2 and Thr<sup>947</sup>-phosphorylated AHA2. The interaction was not regulated by 30 minutes of 100 nM IAA treatment, but the phosphorylation state of the interacting AHA2 was increased.

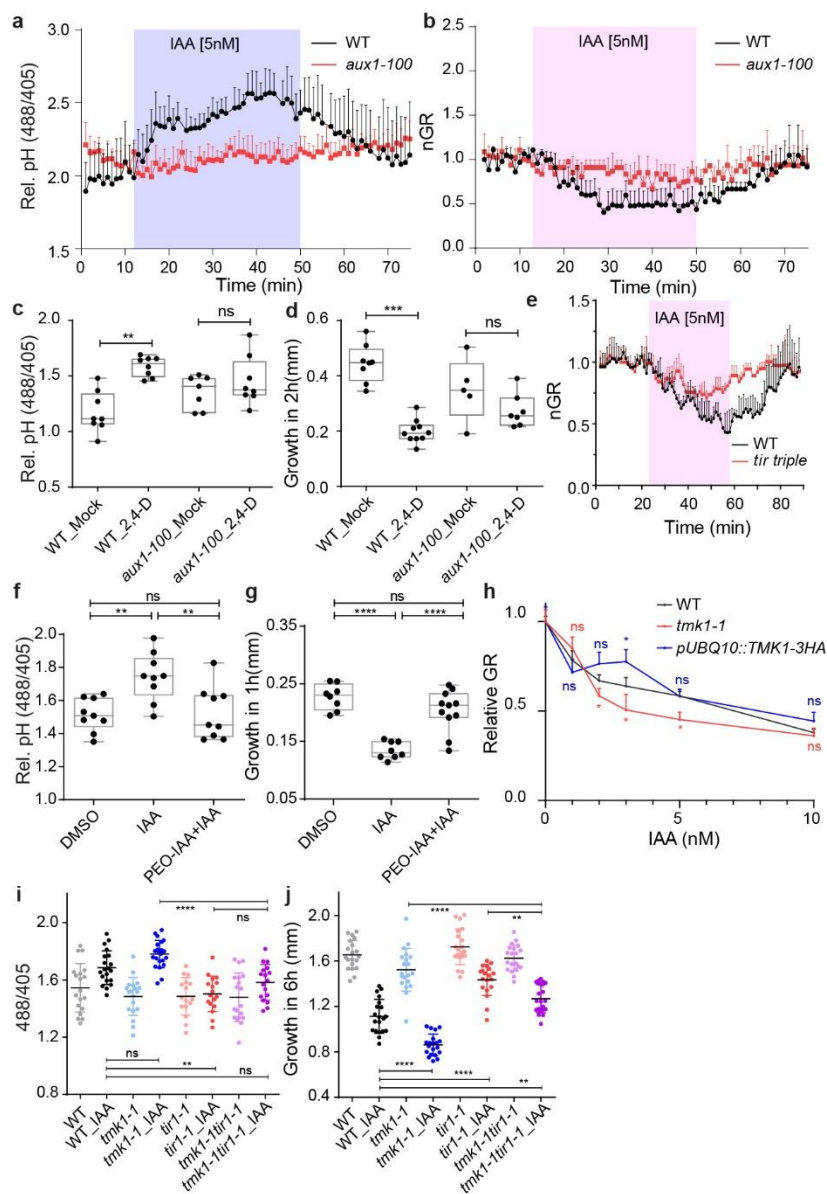
**d**, Bimolecular Fluorescent Complementation (BiFC) in *Nicotiana benthamiana* leaves transiently transformed with *YFP<sup>N</sup>-TMK1*, *AHA2-YFP<sup>C</sup>* or both. Scale bar = 10μm

**e**, Representation of wilting leaves of *Nicotiana benthamiana* that transiently express the WT TMK1 and ATP-site mutated forms: *p35S::TMK1-HA* K<sup>616E</sup> or K<sup>616R</sup>.

**f**, Western blot analysis of the AHA2 levels and the Thr<sup>947</sup> phosphorylation in roots of *DEX::TMK1*<sup>K616R</sup>-HA and *DEX::TMK1-HA* lines treated +/- DEX (30 μM for 24 hours) and +/- IAA (100 nM for 1 hour).

1128 **g-h**, Western blot detection of the AHA2 levels and the Thr<sup>947</sup> phosphorylation in *tmk1,3* roots treated  
1129 with 100 nM IAA for 1 hour (**g**). Quantification of the auxin effect on AHA2 phosphorylation in (**g**) by  
1130 normalising the intensity ratio of pThr<sup>947</sup> to AHA2 detected in auxin-treated roots to the same ratio in  
1131 mock-treated samples of the same genotype (**h**).





# **Extended Data Figure 4. TIR1/AFB and TMK1 signalling converge antagonistically on apoplastic pH and growth regulation.**

**a-b**, Apoplastic alkalisation (**a**) and root growth inhibition (**b**) in response to IAA measured in *aux1-100* mutant compared to WT roots in vRootchip. Apoplastic pH is measured by the HPTS dye.  $n = 3$ ;  $p \leq 0.0001$ , Two-way ANOVA for both graphs.

**c-d**, Apoplastic alkalisation (**c**) and root growth inhibition (**d**) in response to the synthetic auxin analogue 2,4-D in *aux1-100* mutant compared to WT roots. The steady state pH with the HPTS dye was measured 30 minutes after mock or 100 nM 2,4-D treatment.  $n > 6$ , One-way ANOVA (**c**). The growth obtained in 2 hours was captured by scanner.  $n > 4$ , One-way ANOVA (**d**). ns  $p > 0.05$ , \*\* $p \leq 0.01$ , \*\*\* $p \leq 0.001$ .

**e**, Root growth of *tir triple* mutant (in red) compared to WT (in black) in response to 5 nM IAA in the vRootchip.  $n = 3$ , 2.  $p \leq 0.0001$ , two-way ANOVA.

**f-g**, apoplastic pH (**f**) and root growth (**g**) after 10  $\mu$ M PEO-IAA and 5 nM IAA. The steady state pH was measured 30 minutes after the treatments using the HPTS dye, while the root growth obtained in 1 hour was recorded by scanning the plates.  $n > 7$ , ns  $p > 0.05$ , \*\* $p \leq 0.01$ , \*\*\*\* $p \leq 0.0001$ , One-way ANOVA.

1147 **h**, Dose-response of auxin-induced root growth inhibition of *pUBQ10::TMK1-3HA* compared to WT and  
1148 *tmk1-1*. Relative GR is the ratio between auxin-affected growth in a mutant to the mock growth for the  
1149 same genotype. *n* > 7. ns  $p > 0.05$ , \* $p \leq 0.05$ , Welch ANOVA.  
1150 **i-j**, Raw data for **Figure 4d** and **e**, respectively. ns  $p > 0.05$ , \*\* $p \leq 0.01$ , \*\*\*\* $p \leq 0.0001$ , One-way ANOVA.

```

1151 Extended Data Script 1.
1152 import controlP5.*; //import ControlP5 library
1153 import processing.serial.*;
1154 Serial port;
1155 ControlP5 cp5; //create ControlP5 object
1156 PFont font;
1157 void setup(){ //same as arduino program
1158     size(800, 800); //window size, (width, height)
1159     printArray(Serial.list()); //prints all available serial ports
1160     port = new Serial(this, "COM1", 9600);
1161     cp5 = new ControlP5(this);
1162     font = createFont("Times New Roman", 20); // custom fonts for buttons and title
1163     cp5.addButton("DtoW") // "alloff" is the name of button
1164     .setPosition(50, 50) //x and y coordinates of upper left corner of button
1165     .setSize(100, 75) //(width, height)
1166     .setFont(font)
1167     ;
1168     cp5.addButton("CtoW") // "red" is the name of button
1169     .setPosition(50, 150) //x and y coordinates of upper left corner of button
1170     .setSize(100, 75) //(width, height)
1171     .setFont(font)
1172     ;
1173     cp5.addButton("BtoW") // "red" is the name of button
1174     .setPosition(50, 250) //x and y coordinates of upper left corner of button
1175     .setSize(100, 75) //(width, height)
1176     .setFont(font)
1177     ;
1178     cp5.addButton("AtoW") // "red" is the name of button
1179     .setPosition(50, 350) //x and y coordinates of upper left corner of button
1180     .setSize(100, 75) //(width, height)
1181     .setFont(font)
1182     ;
1183     cp5.addButton("Ato78") // "red" is the name of button
1184     .setPosition(175, 50) //x and y coordinates of upper left corner of button
1185     .setSize(100, 75) //(width, height)
1186     .setFont(font)
1187     ;
1188     cp5.addButton("Ato112") // "red" is the name of button
1189     .setPosition(175, 150) //x and y coordinates of upper left corner of button
1190     .setSize(100, 75) //(width, height)
1191     .setFont(font)
1192     ;
1193     cp5.addButton("AtoAll") // "red" is the name of button
1194     .setPosition(350, 50) //x and y coordinates of upper left corner of button
1195     .setSize(100, 75) //(width, height)
1196     .setFont(font)
1197     ;
1198     cp5.addButton("BtoAll") // "red" is the name of button
1199     .setPosition(350, 150) //x and y coordinates of upper left corner of button
1200     .setSize(100, 75) //(width, height)
1201     .setFont(font)

```



```
1202 ;
1203 cp5.addButton("CtoAll")  //"red" is the name of button
1204     .setPosition(350, 250) //x and y coordinates of upper left corner of button
1205     .setSize(100, 75)    //(width, height)
1206     .setFont(font)
1207 ;
1208 cp5.addButton("DtoA")    //"alloff" is the name of button
1209     .setPosition(350, 350) //x and y coordinates of upper left corner of button
1210     .setSize(100, 75)    //(width, height)
1211     .setFont(font)
1212 ;
1213 cp5.addButton("AtoF4")   //"red" is the name of button
1214     .setPosition(475, 50) //x and y coordinates of upper left corner of button
1215     .setSize(100, 75)    //(width, height)
1216     .setFont(font)
1217 ;
1218 cp5.addButton("BtoF4")   //"red" is the name of button
1219     .setPosition(475, 150) //x and y coordinates of upper left corner of button
1220     .setSize(100, 75)    //(width, height)
1221     .setFont(font)
1222 ;
1223 cp5.addButton("CtoF4")   //"red" is the name of button
1224     .setPosition(475, 250) //x and y coordinates of upper left corner of button
1225     .setSize(100, 75)    //(width, height)
1226     .setFont(font)
1227 ;
1228 cp5.addButton("DtoF4")   //"alloff" is the name of button
1229     .setPosition(475, 350) //x and y coordinates of upper left corner of button
1230     .setSize(100, 75)    //(width, height)
1231     .setFont(font)
1232 ;
1233 cp5.addButton("AtoL4")   //"red" is the name of button
1234     .setPosition(600, 50) //x and y coordinates of upper left corner of button
1235     .setSize(100, 75)    //(width, height)
1236     .setFont(font)
1237 ;
1238 cp5.addButton("BtoL4")   //"red" is the name of button
1239     .setPosition(600, 150) //x and y coordinates of upper left corner of button
1240     .setSize(100, 75)    //(width, height)
1241     .setFont(font)
1242 ;
1243 cp5.addButton("CtoL4")   //"red" is the name of button
1244     .setPosition(600, 250) //x and y coordinates of upper left corner of button
1245     .setSize(100, 75)    //(width, height)
1246     .setFont(font)
1247 ;
1248 cp5.addButton("DtoL4")   //"alloff" is the name of button
1249     .setPosition(600, 350) //x and y coordinates of upper left corner of button
1250     .setSize(100, 75)    //(width, height)
1251     .setFont(font)
1252 ;
```

```

1253 cp5.addButton("AllOn")  //"alloff" is the name of button
1254     .setPosition(600, 600) //x and y coordinates of upper left corner of button
1255     .setSize(100, 75)    //(width, height)
1256     .setFont(font)
1257 ;
1258 cp5.addButton("X1")  //"alloff" is the name of button
1259     .setPosition(50, 450) //x and y coordinates of upper left corner of button
1260     .setSize(25, 25)    //(width, height)
1261     .setFont(font)
1262 ;
1263 cp5.addButton("Y1")  //"alloff" is the name of button
1264     .setPosition(50, 500) //x and y coordinates of upper left corner of button
1265     .setSize(25, 25)    //(width, height)
1266     .setFont(font)
1267 ;
1268 cp5.addButton("X2")  //"alloff" is the name of button
1269     .setPosition(85, 450) //x and y coordinates of upper left corner of button
1270     .setSize(25, 25)    //(width, height)
1271     .setFont(font)
1272 ;
1273 cp5.addButton("Y2")  //"alloff" is the name of button
1274     .setPosition(85, 500) //x and y coordinates of upper left corner of button
1275     .setSize(25, 25)    //(width, height)
1276     .setFont(font)
1277 ;
1278 cp5.addButton("X3")  //"alloff" is the name of button
1279     .setPosition(120, 450) //x and y coordinates of upper left corner of button
1280     .setSize(25, 25)    //(width, height)
1281     .setFont(font)
1282 ;
1283 cp5.addButton("Y3")  //"alloff" is the name of button
1284     .setPosition(120, 500) //x and y coordinates of upper left corner of button
1285     .setSize(25, 25)    //(width, height)
1286     .setFont(font)
1287 ;
1288 cp5.addButton("X4")  //"alloff" is the name of button
1289     .setPosition(155, 450) //x and y coordinates of upper left corner of button
1290     .setSize(25, 25)    //(width, height)
1291     .setFont(font)
1292 ;
1293 cp5.addButton("Y4")  //"alloff" is the name of button
1294     .setPosition(155, 500) //x and y coordinates of upper left corner of button
1295     .setSize(25, 25)    //(width, height)
1296     .setFont(font)
1297 ;
1298 cp5.addButton("X5")  //"alloff" is the name of button
1299     .setPosition(190, 450) //x and y coordinates of upper left corner of button
1300     .setSize(25, 25)    //(width, height)
1301     .setFont(font)
1302 ;
1303 cp5.addButton("Y5")  //"alloff" is the name of button

```

```

1304     .setPosition(190, 500) //x and y coordinates of upper left corner of button
1305     .setSize(25, 25)    //(width, height)
1306     .setFont(font)
1307 ;
1308 cp5.addButton("X6")    //"alloff" is the name of button
1309     .setPosition(225, 450) //x and y coordinates of upper left corner of button
1310     .setSize(25, 25)    //(width, height)
1311     .setFont(font)
1312 ;
1313 cp5.addButton("Y6")    //"alloff" is the name of button
1314     .setPosition(225, 500) //x and y coordinates of upper left corner of button
1315     .setSize(25, 25)    //(width, height)
1316     .setFont(font)
1317 ;
1318 cp5.addButton("X7")    //"alloff" is the name of button
1319     .setPosition(260, 450) //x and y coordinates of upper left corner of button
1320     .setSize(25, 25)    //(width, height)
1321     .setFont(font)
1322 ;
1323 cp5.addButton("Y7")    //"alloff" is the name of button
1324     .setPosition(260, 500) //x and y coordinates of upper left corner of button
1325     .setSize(25, 25)    //(width, height)
1326     .setFont(font)
1327 ;
1328 cp5.addButton("X8")    //"alloff" is the name of button
1329     .setPosition(295, 450) //x and y coordinates of upper left corner of button
1330     .setSize(25, 25)    //(width, height)
1331     .setFont(font)
1332 ;
1333 cp5.addButton("Y8")    //"alloff" is the name of button
1334     .setPosition(295, 500) //x and y coordinates of upper left corner of button
1335     .setSize(25, 25)    //(width, height)
1336     .setFont(font)
1337 ;
1338 cp5.addButton("X9")    //"alloff" is the name of button
1339     .setPosition(330, 450) //x and y coordinates of upper left corner of button
1340     .setSize(25, 25)    //(width, height)
1341     .setFont(font)
1342 ;
1343 cp5.addButton("Y9")    //"alloff" is the name of button
1344     .setPosition(330, 500) //x and y coordinates of upper left corner of button
1345     .setSize(25, 25)    //(width, height)
1346     .setFont(font)
1347 ;
1348 cp5.addButton("X10")   //"alloff" is the name of button
1349     .setPosition(365, 450) //x and y coordinates of upper left corner of button
1350     .setSize(40, 25)    //(width, height)
1351     .setFont(font)
1352 ;
1353 cp5.addButton("Y10")   //"alloff" is the name of button
1354     .setPosition(365, 500) //x and y coordinates of upper left corner of button

```

```

1355     .setSize(40, 25)    //(width, height)
1356     .setFont(font)
1357 ;
1358 cp5.addButton("X11")    //"alloff" is the name of button
1359     .setPosition(415, 450) //x and y coordinates of upper left corner of button
1360     .setSize(40, 25)    //(width, height)
1361     .setFont(font)
1362 ;
1363 cp5.addButton("Y11")    //"alloff" is the name of button
1364     .setPosition(415, 500) //x and y coordinates of upper left corner of button
1365     .setSize(40, 25)    //(width, height)
1366     .setFont(font)
1367 ;
1368 cp5.addButton("X12")    //"alloff" is the name of button
1369     .setPosition(465, 450) //x and y coordinates of upper left corner of button
1370     .setSize(40, 25)    //(width, height)
1371     .setFont(font)
1372 ;
1373 cp5.addButton("Y12")    //"alloff" is the name of button
1374     .setPosition(465, 500) //x and y coordinates of upper left corner of button
1375     .setSize(40, 25)    //(width, height)
1376     .setFont(font)
1377 ;
1378 }
1379 void draw(){ //same as loop in arduino
1380     background(150, 0 , 150); // background color of window (r, g, b) or (0 to 255)
1381
1382     //lets give title to our window
1383     fill(0, 255, 0);          //text color (r, g, b)
1384     textFont(font);
1385     text("VALVE CONTROL", 50, 30); // ("text", x coordinate, y coordinat)
1386 }
1387 void CtoW(){
1388     port.write('a');
1389 }
1390 void BtoW(){
1391     port.write('b');
1392 }
1393 void AtoW(){
1394     port.write('c');
1395 }
1396 void Ato78(){
1397     port.write('d');
1398 }
1399 void Ato1112(){
1400     port.write('e');
1401 }
1402 void AtoAll(){
1403     port.write('f');
1404 }
1405 void BtoAll(){

```

```
1406     port.write('g');
1407 }
1408 void CtoAll(){
1409     port.write('h');
1410 }
1411 void AtoF4(){
1412     port.write('i');
1413 }
1414 void BtoF4(){
1415     port.write('j');
1416 }
1417 void CtoF4(){
1418     port.write('k');
1419 }
1420 void AtoL4(){
1421     port.write('l');
1422 }
1423 void BtoL4(){
1424     port.write('m');
1425 }
1426 void CtoL4(){
1427     port.write('n');
1428 }
1429 void AllOn(){
1430     port.write('o');
1431 }
1432 void DtoW(){
1433     port.write('p');
1434 }
1435 void DtoA(){
1436     port.write('q');
1437 }
1438 void DtoF4(){
1439     port.write('r');
1440 }
1441 void DtoL4(){
1442     port.write('s');
1443 }
1444 void X1(){
1445     port.write('A');
1446 }
1447 void X2(){
1448     port.write('B');
1449 }
1450 void X3(){
1451     port.write('C');
1452 }
1453 void X4(){
1454     port.write('D');
1455 }
1456 void X5(){
```

```
1457     port.write('E');
1458 }
1459 void X6(){
1460     port.write('F');
1461 }
1462 void X7(){
1463     port.write('G');
1464 }
1465 void X8(){
1466     port.write('H');
1467 }
1468 void X9(){
1469     port.write('I');
1470 }
1471 void X10(){
1472     port.write('J');
1473 }
1474 void X11(){
1475     port.write('K');
1476 }
1477 void X12(){
1478     port.write('L');
1479 }
1480 void Y1(){
1481     port.write('M');
1482 }
1483 void Y2(){
1484     port.write('N');
1485 }
1486 void Y3(){
1487     port.write('O');
1488 }
1489 void Y4(){
1490     port.write('P');
1491 }
1492 void Y5(){
1493     port.write('Q');
1494 }
1495 void Y6(){
1496     port.write('R');
1497 }
1498 void Y7(){
1499     port.write('S');
1500 }
1501 void Y8(){
1502     port.write('T');
1503 }
1504 void Y9(){
1505     port.write('U');
1506 }
1507 void Y10(){
```

```

1508     port.write('V');
1509 }
1510 void Y11(){
1511     port.write('W');
1512 }
1513 void Y12(){
1514     port.write('X');
1515 }
1516
1517 Extended Data Script 2.
1518 int incomingByte = 0;
1519 int p1 = 1;int p2 = 2;int p3 = 3;int p4 = 4;int p5 = 5;int p6 = 6;int p7 = 7;int p8 = 8;int p9 = 9;int p10 =
1520 10;int p11 = 11;int p12 = 12;int p13 = 13;int p14 = 14;int p15 = 15;int p16 = 16;int p17 = 17;int p18 =
1521 18;int p19 = 19;int p20 = 20;int p21 = 21;int p22 = 22;int p23 = 23;int p24 = 24;
1522
1523 void setallvalves(int v1, int v2, int v3, int v4, int v5, int v6, int v7, int v8, int v9, int v10, int v11, int v12,
1524 int v13, int v14, int v15, int v16, int v17, int v18, int v19, int v20, int v21, int v22, int v23, int v24){
1525     if (v1 == 1){digitalWrite(p1, HIGH);}
1526     else {digitalWrite(p1, LOW);}
1527     if (v2 == 1){digitalWrite(p2, HIGH);}
1528     else {digitalWrite(p2, LOW);}
1529     if (v3 == 1){digitalWrite(p3, HIGH);}
1530     else{digitalWrite(p3, LOW);}
1531     if (v4 == 1){digitalWrite(p4, HIGH);}
1532     else{digitalWrite(p4, LOW);}
1533     if (v5 == 1){digitalWrite(p5, HIGH);}
1534     else{digitalWrite(p5, LOW);}
1535     if (v6 == 1){digitalWrite(p6, HIGH);}
1536     else{digitalWrite(p6, LOW);}
1537     if (v7 == 1){digitalWrite(p7, HIGH);}
1538     else{digitalWrite(p7, LOW);}
1539     if (v8 == 1){digitalWrite(p8, HIGH);}
1540     else{digitalWrite(p8, LOW);}
1541     if (v9 == 1){digitalWrite(p9, HIGH);}
1542     else{digitalWrite(p9, LOW);}
1543     if (v10 == 1){digitalWrite(p10, HIGH);}
1544     else{digitalWrite(p10, LOW);}
1545     if (v11 == 1){digitalWrite(p11, HIGH);}
1546     else{digitalWrite(p11, LOW);}
1547     if (v12 == 1){digitalWrite(p12, HIGH);}
1548     else{digitalWrite(p12, LOW);}
1549     if (v13 == 1){digitalWrite(p13, HIGH);}
1550     else{digitalWrite(p13, LOW);}
1551     if (v14 == 1){digitalWrite(p14, HIGH);}
1552     else{digitalWrite(p14, LOW);}
1553     if (v15 == 1){digitalWrite(p15, HIGH);}
1554     else{digitalWrite(p15, LOW);}
1555     if (v16 == 1){digitalWrite(p16, HIGH);}
1556     else{digitalWrite(p16, LOW);}
1557     if (v17 == 1){digitalWrite(p17, HIGH);}
1558     else{digitalWrite(p17, LOW);}

```

```

1559     if (v18 == 1){digitalWrite(p18, HIGH);}
1560     else{digitalWrite(p18, LOW);}
1561     if (v19 == 1){digitalWrite(p19, HIGH);}
1562     else{digitalWrite(p19, LOW);}
1563     if (v20 == 1){digitalWrite(p20, HIGH);}
1564     else{digitalWrite(p20, LOW);}
1565     if (v21 == 1){digitalWrite(p21, HIGH);}
1566     else{digitalWrite(p21, LOW);}
1567     if (v22 == 1){digitalWrite(p22, HIGH);}
1568     else{digitalWrite(p22, LOW);}
1569     if (v23 == 1){digitalWrite(p23, HIGH);}
1570     else{digitalWrite(p23, LOW);}
1571     if (v24 == 1){digitalWrite(p24, HIGH);}
1572     else{digitalWrite(p24, LOW);}
1573 }
1574
1575 void setup() {
1576     Serial.begin(9600);
1577     pinMode(p1, OUTPUT);pinMode(p2, OUTPUT);pinMode(p3, OUTPUT);pinMode(p4,
1578 OUTPUT);pinMode(p5, OUTPUT);pinMode(p6, OUTPUT); pinMode(p7, OUTPUT); pinMode(p8,
1579 OUTPUT); pinMode(p9, OUTPUT); pinMode(p10, OUTPUT); pinMode(p11, OUTPUT);
1580 pinMode(p12, OUTPUT); pinMode(p13, OUTPUT); pinMode(p14, OUTPUT); pinMode(p15,
1581 OUTPUT); pinMode(p16, OUTPUT); pinMode(p17, OUTPUT); pinMode(p18, OUTPUT);
1582 pinMode(p19, OUTPUT); pinMode(p20, OUTPUT); pinMode(p21, OUTPUT); pinMode(p22,
1583 OUTPUT);pinMode(p23, OUTPUT);pinMode(p24, OUTPUT);
1584     delay(1000);
1585     digitalWrite(p1, LOW); digitalWrite(p2, LOW); digitalWrite(p3, LOW); digitalWrite(p4, LOW);
1586     digitalWrite(p5, LOW);digitalWrite(p6, LOW); digitalWrite(p7, LOW); digitalWrite(p8, LOW);
1587     digitalWrite(p9, LOW); digitalWrite(p10, LOW); digitalWrite(p11, LOW); digitalWrite(p12, LOW);
1588     digitalWrite(p13, LOW); digitalWrite(p14, LOW); digitalWrite(p15, LOW); digitalWrite(p16, LOW);
1589     digitalWrite(p17, LOW); digitalWrite(p18, LOW); digitalWrite(p19, LOW); digitalWrite(p20, LOW);
1590     digitalWrite(p21, LOW); digitalWrite(p22, LOW); digitalWrite(p23, LOW); digitalWrite(p24, LOW);
1591 }
1592
1593 void loop() {
1594     // if we get a valid byte, read analog ins:
1595     if (Serial.available() > 0) {
1596         // get incoming byte:
1597         char val = Serial.read();
1598         if(val == 'a'){ //C -> Waste
1599             setallvalves(1,0,0,1,0,0,1,1,1,1,1,0,0,0,0,0,0,0,0,0,0,0);
1600         }
1601         if(val == 'b'){ //B -> Waste
1602             setallvalves(0,1,1,0,0,0,1,1,1,1,1,0,0,0,0,0,0,0,0,0,0,0);
1603         }
1604         if(val == 'c'){ //A -> Waste
1605             setallvalves(1,0,1,0,0,0,1,1,1,1,1,0,0,0,0,0,0,0,0,0,0,0);
1606         }
1607         if(val == 'd'){ //A -> 7,8
1608             setallvalves(1,0,1,0,1,0,1,1,1,1,1,0,0,0,0,0,0,0,0,0,0,0);
1609         }

```



```

1610 if(val == 'e'){ //A -> 11,12
1611     setallvalves(1,0,1,0,1,0,0,0,0,0,1,1,0,0,0,0,0,0,0,0,0,0);
1612 }
1613 if(val == 'f'){ //A -> All
1614     setallvalves(1,0,1,0,1,0,0,0,0,0,0,0,0,0,0,0,0,0,0,0,0,0);
1615 }
1616 if(val == 'g'){ //B -> All
1617     setallvalves(0,1,1,0,1,0,0,0,0,0,0,0,0,0,0,0,0,0,0,0,0,0);
1618 }
1619 if(val == 'h'){ //C -> All
1620     setallvalves(1,0,0,1,1,0,0,0,0,0,0,0,0,0,0,0,0,0,0,0,0,0);
1621 }
1622 if(val == 'i'){ //A -> First 4
1623     setallvalves(1,0,1,0,1,0,0,1,0,0,0,0,0,0,0,0,0,0,0,0,0,0);
1624 }
1625 if(val == 'j'){ //B -> First 4
1626     setallvalves(0,1,1,0,1,0,0,1,0,0,0,0,0,0,0,0,0,0,0,0,0,0);
1627 }
1628 if(val == 'k'){ //C -> First 4
1629     setallvalves(1,0,0,1,1,0,0,1,0,0,0,0,0,0,0,0,0,0,0,0,0,0);
1630 }
1631 if(val == 'l'){ //A -> Last 4
1632     setallvalves(1,0,1,0,1,0,1,0,0,0,0,0,0,0,0,0,0,0,0,0,0,0);
1633 }
1634 if(val == 'm'){ //B -> Last 4
1635     setallvalves(0,1,1,0,1,0,1,0,0,0,0,0,0,0,0,0,0,0,0,0,0,0);
1636 }
1637 if(val == 'n'){ //C -> Last 4
1638     setallvalves(1,0,0,1,1,0,1,0,0,0,0,0,0,0,0,0,0,0,0,0,0,0);
1639 }
1640 if(val == 'o'){ //All On
1641     setallvalves(1,1,1,1,1,1,1,1,1,1,1,0,0,0,0,0,0,0,0,0,0,0);
1642 }
1643
1644 if(val == 'p'){ //D to Waste
1645     setallvalves(0,1,0,1,0,0,1,1,1,1,1,1,0,0,0,0,0,0,0,0,0,0);
1646 }
1647 if(val == 'q'){ //D to All
1648     setallvalves(0,1,0,1,1,0,0,0,0,0,0,0,0,0,0,0,0,0,0,0,0,0);
1649 }
1650 if(val == 'r'){ //D to Former 4
1651     setallvalves(0,1,0,1,1,0,0,1,0,0,0,0,0,0,0,0,0,0,0,0,0,0);
1652 }
1653 if(val == 's'){ //D to Later 4
1654     setallvalves(0,1,0,1,1,0,1,0,0,0,0,0,0,0,0,0,0,0,0,0,0,0);
1655 }
1656
1657 if(val == 'A'){ //V1 On
1658     digitalWrite(p1, HIGH);
1659 }
1660 if(val == 'B'){ //V2 On

```

```
1661     digitalWrite(p2, HIGH);
1662     }
1663     if(val == 'C'){    //V3 On
1664         digitalWrite(p3, HIGH);
1665     }
1666     if(val == 'D'){    //V4 On
1667         digitalWrite(p4, HIGH);
1668     }
1669     if(val == 'E'){    //V5 On
1670         digitalWrite(p5, HIGH);
1671     }
1672     if(val == 'F'){    //V6 On
1673         digitalWrite(p6, HIGH);
1674     }
1675     if(val == 'G'){    //V7 On
1676         digitalWrite(p7, HIGH);
1677     }
1678     if(val == 'H'){    //V8 On
1679         digitalWrite(p8, HIGH);
1680     }
1681     if(val == 'I'){    //V9 On
1682         digitalWrite(p9, HIGH);
1683     }
1684     if(val == 'J'){    //V10 On
1685         digitalWrite(p10, HIGH);
1686     }
1687     if(val == 'K'){    //V11 On
1688         digitalWrite(p11, HIGH);
1689     }
1690     if(val == 'L'){    //V12 On
1691         digitalWrite(p12, HIGH);
1692     }
1693     if(val == 'M'){    //V1 Off
1694         digitalWrite(p1, LOW);
1695     }
1696     if(val == 'N'){    //V2 Off
1697         digitalWrite(p2, LOW);
1698     }
1699     if(val == 'O'){    //V3 Off
1700         digitalWrite(p3, LOW);
1701     }
1702     if(val == 'P'){    //V4 Off
1703         digitalWrite(p4, LOW);
1704     }
1705     if(val == 'Q'){    //V5 Off
1706         digitalWrite(p5, LOW);
1707     }
1708     if(val == 'R'){    //V6 Off
1709         digitalWrite(p6, LOW);
1710     }
1711     if(val == 'S'){    //V7 Off
```

```
1712     digitalWrite(p7, LOW);
1713     }
1714     if(val == 'T'){    //V8 Off
1715         digitalWrite(p8, LOW);
1716     }
1717     if(val == 'U'){    //V9 Off
1718         digitalWrite(p9, LOW);
1719     }
1720     if(val == 'V'){    //V10 Off
1721         digitalWrite(p10, LOW);
1722     }
1723     if(val == 'W'){    //V11 Off
1724         digitalWrite(p11, LOW);
1725     }
1726     if(val == 'X'){    //V12 Off
1727         digitalWrite(p12, LOW);
1728     }
1729 }
1730 }
```